Instrument Science Report STIS 2015-09

Summary of the STIS Cycle 21 Calibration Program

Hugues Sana, Andrew Fox, Julia Roman-Duval, Justin Ely, Colin Cox, Audrey DiFelice, Svea Hernandez, Sean Lockwood, Cristina Oliveira, Steve Penton, Charles Proffitt, David Sahnow, Paule Sonnentrucker, Jo Taylor, Alan D. Welty, Thomas Wheeler

September 25, 2015

ABSTRACT

We summarize the Cycle 21 calibration program for the Space Telescope Imaging Spectrograph (STIS) on the Hubble Space Telescope covering the time period November 2013 through October 2014. We give an overview of the whole program, and status summaries for each of the individual proposals comprising the program.

1. Introduction

The Space Telescope Imaging Spectrograph (STIS) on the Hubble Space Telescope was repaired in May 2009. Cycle 21 was the fifth cycle of on-orbit post-repair STIS operations. The calibration program for this period resembles the typical calibration and monitoring programs of the mature STIS instrument prior to its failure in 2004, with fewer special calibrations than had been included in the Cycle 17 STIS calibration program. Cycle 21 observations commenced in November 2012 and ran through October 2013.

In this document we record and summarize the results of the individual calibration programs. Section 2 gives a summary and overview of the calibration program, which comprises 22 unique programs. Most of these are regular programs to monitor and track instrument performance. There was one special calibration program devoted to measuring the STIS CCD saturation limits (PID 13545) and one contingency program (13553).

Section 3 of this document details results from individual programs. The **Error! Reference source not found.** lists reference files and documentation produced as a result of Cycle 21

calibration programs.

2. Overview of calibration proposals for Cycle 21

Table 1 summarizes the orbit allocation and usage during the regular and special Cycle 21 calibration program. No supplemental (special) calibration programs beyond those proposed as the initial calibration plan were required for STIS in this cycle.

Table 1. Summary of orbit allocation and usage during Cycle 21 STIS Calibration

	External Orbits		Internal+parallel orbits	
	Regular	Special	Regular	Special
Allocated	21	0	1387+6[C]	5
Executed	20	0	1387	5
Withdrawn	0	0	0	0
Failed	3	0	0	0
Repeated	3	0	0	0

The calibration monitoring programs in Cycle 21 are essentially continuations of the monitoring programs from the previous cycle. These include programs which assess the stability of the CCD: its read out noise, spurious charge, charge transfer efficiency (CTE), and growth of hot pixels, and which also provide daily dark frames and bias frames for data processing and reduction. Other programs monitor the slit wheel repeatability, CCD and MAMA dispersion solutions, the MAMA focus, the MAMA fold distribution (i.e., the pulse-height distribution), and the sensitivity of both the CCD and MAMA detectors. For these programs, reference files are updated only as needed to maintain calibration within the required levels of accuracy.

Currently available reference files can be found at:
www.stsci.edu/hst/observatory/cdbs/SIfileInfo/STIS/reftablequeryindex Other products resulting from the calibration program include STIS Instrument Science Reports (ISRs), STIS Technical Instrument Reports (TIRs), and updates to the STIS Instrument (IHB) and Data (DHB) Handbooks. Links to these documents can be found at:
www.stsci.edu/hst/stis/documents. Note that TIRs are only available on the internal STScI web site. In order to retrieve TIRs from outside the STScI, a document request needs to be sent to: help@stsci.edu

Table 2 provides a high level summary of the calibration programs, noting specifically products and accuracy achieved. The first two columns give the Proposal ID and its title; columns 3 and 4 give the number of executed [allocated] orbits for each proposal, divided into external and internal orbits. Column 5 gives the frequency of visits for monitoring programs. Column 6 describes the resulting products. For several programs, regularly updated reference files are produced. For many others, results are either posted on the web, or simply documented in Section 3 of this report. Column 7 gives the accuracy achieved by the calibration proposal. The last column of Table 2 notes the page in this ISR on which detailed information for that program can be found.

3. Results from individual proposals

The following sections summarize the purpose, status, and results from the individual calibration proposals in the Cycle 21 program.

Table 2. Overview of Cycle 21 STIS Calibrations Programs.

PID	Title	Orbits used Executed [Allocated]		Frequency	Products	Accuracy achieved	Page
		External	Internal				
CCD Monitors							
13534	**CCD Performance Monitor**	0	14[14]	2x7	Reference file	5% (RN) <1% (G)	5
13518	**CCD Dark Monitor Part I**	0	364[364]	364x1	Reference files	S/N~1.36	7
13519	**CCD Dark Monitor Part II**	0	366[366]	366x1	Reference files	S/N~1.36	7
13535	**CCD Bias and Readnoise Monitor Part I**	0	182[182]	182x1	Reference files	S/N~1.1-2.0	9
13536	**CCD Bias and Readnoise Monitor Part II**	0	187[187]	187x1	Reference files	S/N~1.1-2.0	9
13537	**CCD Hot Pixel Annealing**	0	39[39]	13x3	Webpage updates	See details in report	12
13538	**CCD Spectroscopic Flats**	0	19[19]	various	Reported in this ISR	<1.1% residual scatter	14
13539	**CCD Imaging Flats**	0	4[4]	various	Reported in this ISR	<0.2% residual scatter	15
13540	**CCD Spectroscopic Dispersion Solution Monitor**	0	3[3]	3x1	ISR in prep	Zero-points vary w/ rms <0.35 pixel	17
13541	**CCD Sparse Field CTE**	0	82+x^{H}[82]		Reported in this ISR	<1% for >200 e−	21
13542	**CCD Full Field Sensitivity**	1[1]	0	1x1	ISR	<1%	22
13543	**Slit Wheel Repeatability**	0	1[1]	1x1	Reported in this ISR	Repeatable to 0.013 pixel	25
13544	**CCD Spectroscopic Sensitivity Monitor**	5+1^{H}[5]	0	3x1/L,1x2/M	Reported in this ISR	<1% in rel. flux	26
MAMA Monitors							
13546	**MAMA Dispersion Solution**	0	7[7]	7x1	ISR in prep	Zero-points vary w/ rms <0.35 pixel	31
13547	**MAMA Full Field Sensitivity**	3[3]	0	1x3	ISR	FUV-MAMA: <1% NUV-MAMA: <1%	35
13548	**MAMA Spectroscopic Sensitivity**	12+2^{H}[12]	0	3x1/L, 1x1/M, 4x2/E	TDS reference file + ISR	<2% /E, 0.2-0.5%/L,M	38
13549	**FUV MAMA Dark Monitor**	0	54[54]	2x6	Reported in this ISR	5-10%	41
13550	**NUV MAMA Dark Monitor**	0	52[52]	2/det/alt wks+	Reported in this ISR	5-10%	43
13551	**MAMA NUV Flats**	0	11[11]	Odd cycles	Reported in this ISR	2% residual scatter	45
13552	**MAMA Fold Distribution**	0	2[2]	1x2	Reported in this ISR	~5%	50
Special Calibration programs							
13545	**CCD Saturation Limits**	0	4[4]	???			53
Contingency programs							
13553	**MAMA Anomalous Recovery**	0	0[6]	contingency	N/A	N/A	--

^{C} Contingency orbits, ^{P} Parallel orbits, ^{H} HOPR

Proposal ID 13534: CCD Performance Monitor

(PI: Svea Hernandez)

Analysis Lead, Others: Jo Taylor

Summary of Goals and program design

This program measures the baseline performance of the CCD on STIS. It collects a series of biases and flats at different gains, in order to estimate the read noise, CCD gain, spurious charge and relative measures of charge transfer inefficiency (CTI) from the extended pixel edge response test (EPER).

Execution

Execution was nominal. The program was scheduled to execute two times during Cycle 21. Observations were taken in March 2014 and six months later in September 2014. Each execution consisted of 7 internal orbits.

Summary of Analysis and Results

The analysis was the same as for previous cycles. A more detailed description of this analysis can be found in STIS ISR 2009-02. The overall performance of the STIS CCD continued to be stable. The spurious charge remained constant throughout Cycle 21. Figure 1and Figure 2 present the spurious charge measured at CCDGAIN = 1 and CCDGAIN = 4 respectively. All of these exposures used CCDAMP = D. The extended pixel edge response (EPER) test measured the charge in the overscan bias level using flat fields. This test provided a relative measure of the CTI in the parallel and serial direction. Such measurements reflect an increase in CTI in both directions for Cycle 21, as shown in Figure 3. The CTI in the parallel direction experienced an increase of 10.3% from March to September 2014. The CTI in the serial direction experienced an increase of -5.0% from March to September 2014. The CTI values in the serial direction continue to be one order of magnitude lower then the ones in the parallel direction.

Accuracy Achieved

Read noise error is <0.4 e- or <5% for all different gains. The error in the gain estimates is <0.08 e- or <1%. The read noise and gain errors are higher than the accuracy stated in the Phase I.

Reference Files Delivered

None

Relevant ISRs

None

Continuation Plans

Program continued in Cycle 22 as 13979. No significant changes have been made to the structure of the program for Cycle 22.

Supporting Details

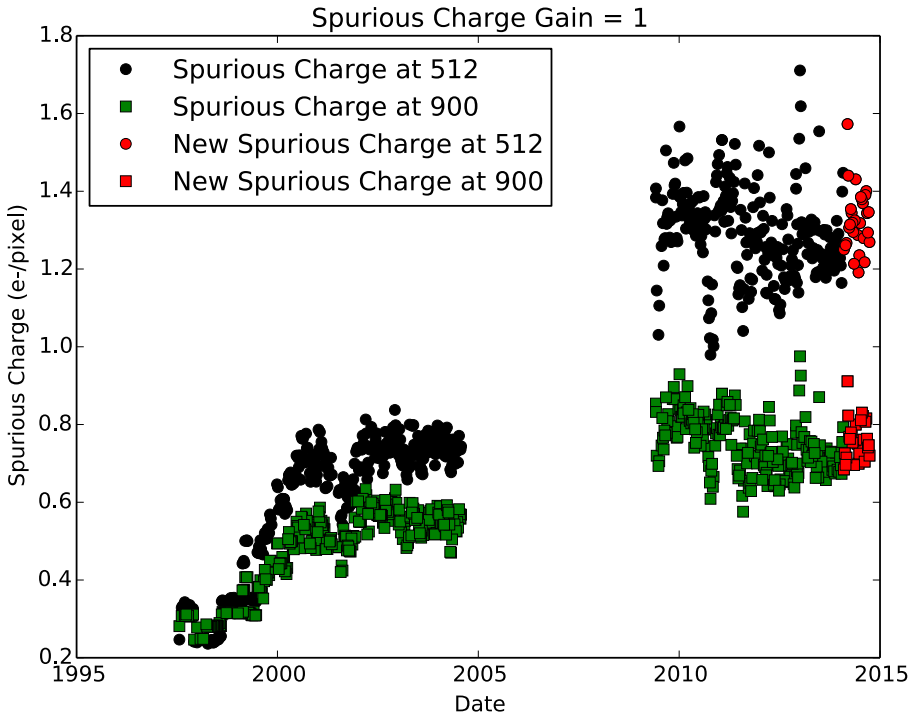

Figure 1. History of the spurious charge measured at the top and center of the CCD chip at CCDGAIN = 1

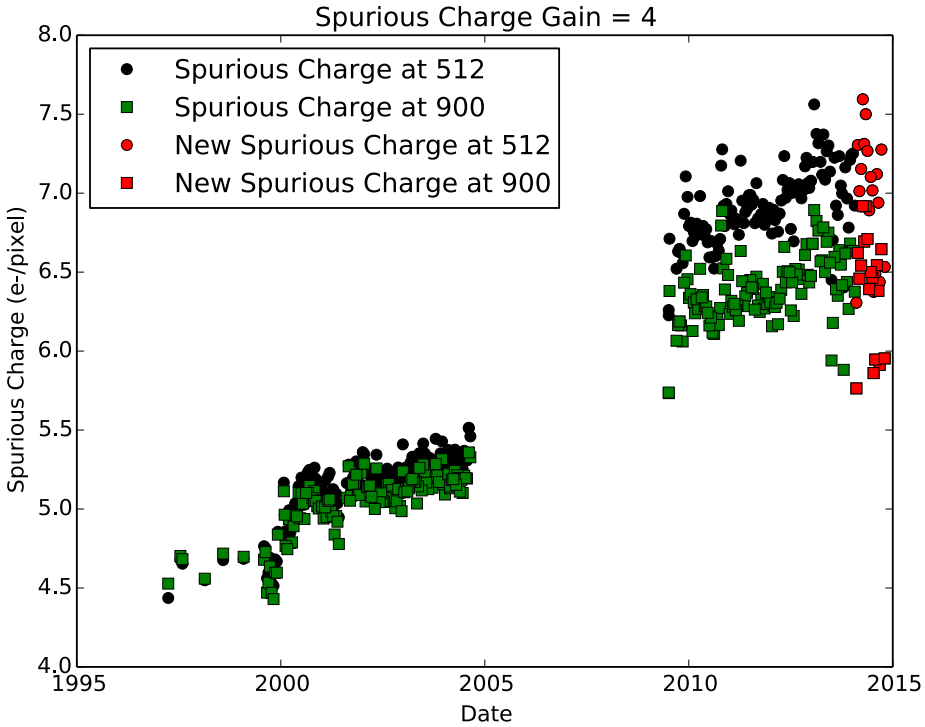

Figure 2. History of the spurious charge measured at the top and center of the CCD chip at CCDGAIN = 4

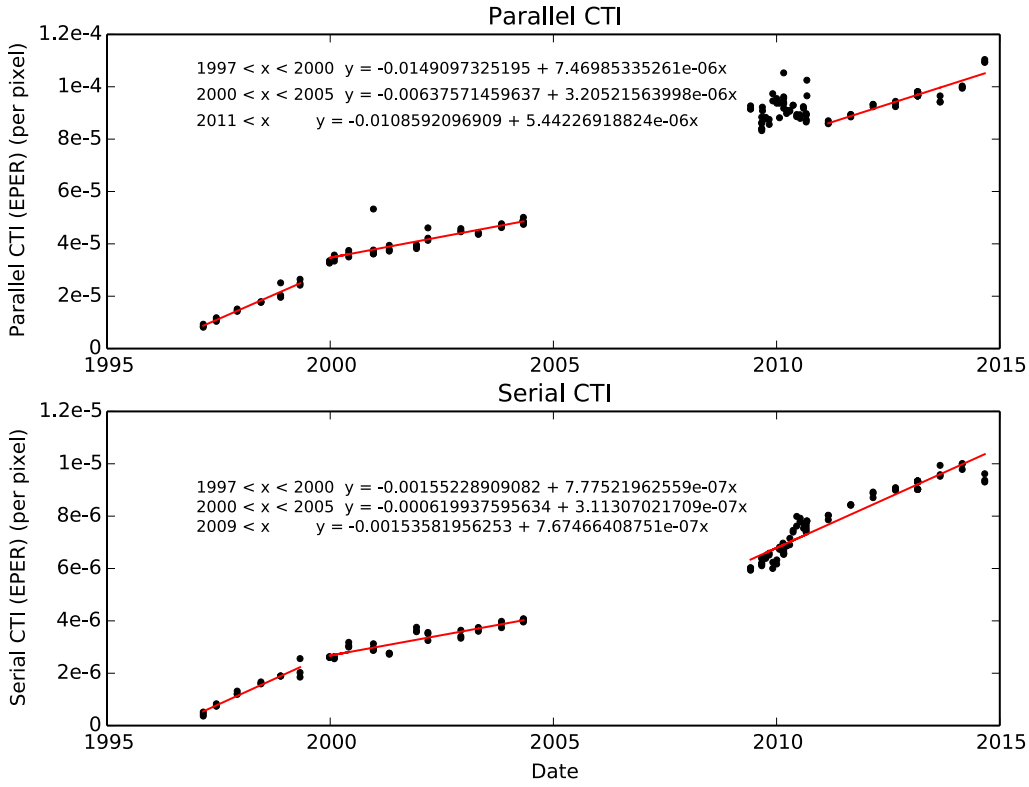

Figure 3. CTI time dependence. Top plot presents the time dependence of the measured EPER CTI in the parallel direction. Bottom plot shows the time dependence of the CTI in the serial direction. The CTI in the parallel direction increased while the serial direction decreased.

Proposal ID 13518 & 13519: CCD Dark Monitor Part I & II

(PI: Svea Hernandez)

Analysis Lead, Others: Jo Taylor

Summary of Goals and program design

The program was designed to produce weekly dark reference files from a series of long dark exposures (1100s). Additionally, short dark exposures are taken daily and are available to observers for updating the hot pixel intensities in the weekly dark reference files. The program obtained darks at CCDGAIN = 1 in order to monitor the CCD behavior and chart growth of hot and bad pixels.

Execution

All 364 internal orbits were executed successfully for both programs.

Summary of Analysis and Results

Darks taken between anneal periods are combined to produce a dark reference image (superdark). In the process of creating these baseline dark images, we made use of the superbiases for the corresponding time range to remove the bias from the dark reference frame. The median dark current for the period of November 2013 to October 2014 was estimated to be 0.01662 e-/s. The average dark current for the same period was estimated to be 0.07498 e-/s. As in previous cycles, the dark current continues to increase. Figure 4 presents the median dark current history of the CCD as a function of time.

Accuracy Achieved

The signal-to-noise achieved on every superdark was ≈1.36, which agrees with the accuracy stated in the Phase I.

Reference Files Delivered

Approximately four superdarks were delivered each anneal period.

Relevant ISRs

None

Continuation Plans

These two programs continued in Cycle 22 with PIDs 13980 and 13981. No significant changes have been made to the structure of the programs for Cycle 22.

Supporting Details

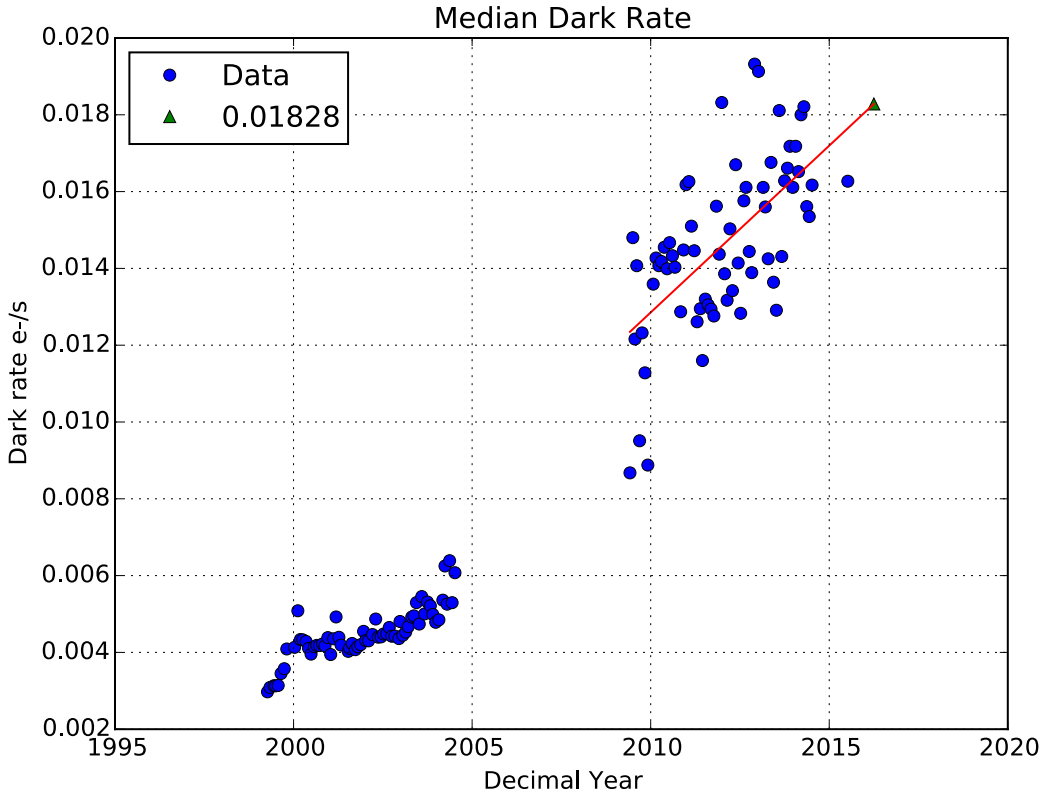

Figure 4. Dark rate vs. time with the slope identified as 0.01828.

Proposal ID 13535 & 13536: CCD Bias and Readnoise Monitor Part I & II
(PI: Svea Hernandez)

Analysis Lead, Others: Jo Taylor

Summary of Goals and program design

One of the main objectives of this program was to monitor the read noise including growth and possible fluctuations for CCDGAIN = 1 and CCDGAIN = 4 in the 1x1 bin setting read out through the nominal amplifier, D. Full frame biases were taken and read out through amplifiers A and C and used in combination with biases taken through amplifier D in order to estimate the detector's read noise. The data taken between monthly anneals was combined weekly (CCDGAIN = 1) or bi-weekly (CCDGAIN=4) to produce reference files.

Execution

Execution was nominal.

Summary of Analysis and Results

Data taken between monthly anneals is combined weekly for CCDGAIN = 1 and biweekly for CCDGAIN = 4 to produce bias reference files. The superbiases produced have a signal-to-noise (S/N) > 1.0. The CCD read noise was estimated by measuring the RMS dispersion in a difference image previously cleaned of discordant pixels via iterative sigma clipping. These values were then plotted and compared to previous measurements in order to better monitor the read noise stability. Figure 5 and Figure 6 present the CCD read noise history of STIS for CCDGAIN = 1 and CCDGAIN = 4 respectively. In May 2014, the readnoise for the CCDGAIN = 1, 1x1 binning, AMP = D setting increased by ~8.5%, and has remained at an elevated level since. This increase is due to the hardware degrading, possibly due to radiation damage. The jump has not been correlated with any new noise sources in STIS or HST, or any sources outside of the STIS CCD electronics.

The average value of the Cycle 21 readnoise is 5.93 ADUs for CCDGAIN = 1 and 2.08 ADUs for CCDGAIN = 4.

Accuracy Achieved

Read noise error is <0.4 e- or <5% for all different gains. The error in the gain estimates is <0.08 e- or <1%. The read noise and gain errors are higher than the accuracy stated in the Phase I.

Reference Files Delivered

Approximately six superbiases were delivered each anneal period, four for CCDGAIN = 1 and two for CCDGAIN = 4.

Relevant ISRs: None

Continuation Plans

These two programs continued in Cycle 22 with PIDs 13982 and 13983. No significant changes have been made to the structure of the programs for Cycle 22.

Supporting Details

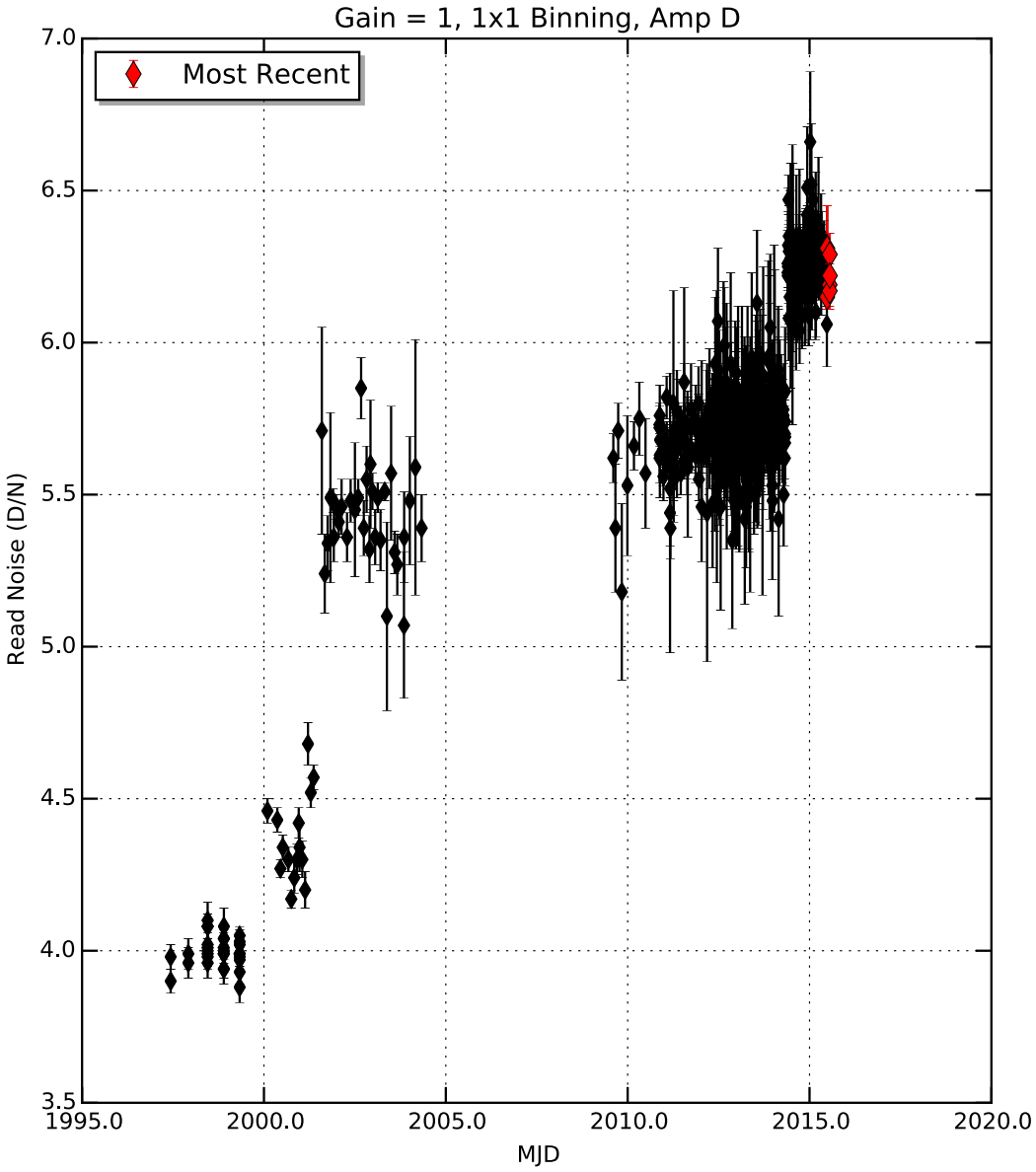

Figure 5. Read noise history for the STIS CCD at CCDGAIN = 1, 1x1 binning and read through amplifier D.

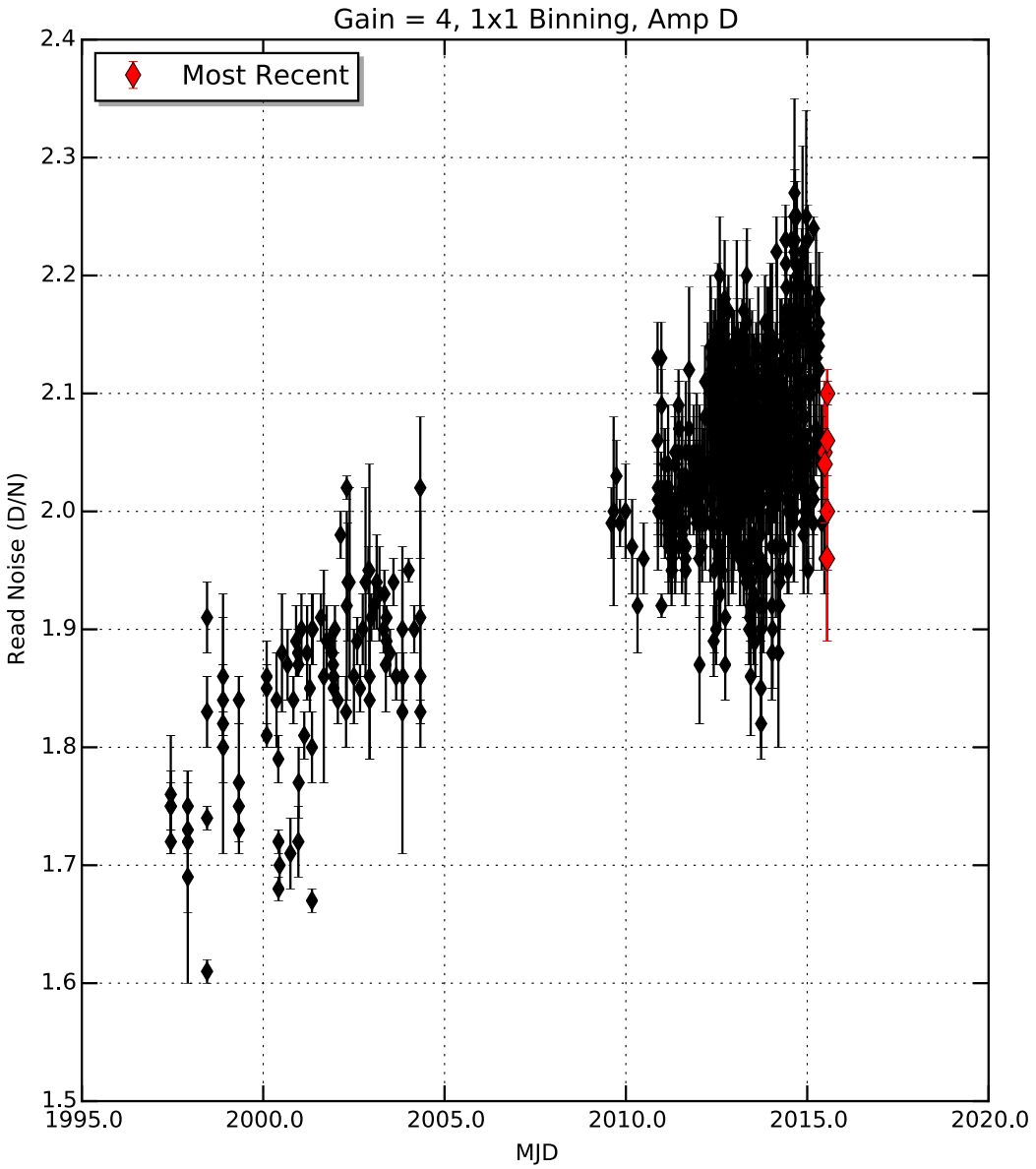

Figure 6. Read noise history for the STIS CCD at CCDGAIN = 4, 1x1 binning and read through amplifier D.

Proposal ID 13537: CCD Hot Pixel Annealing

(PI: Svea Hernandez)

Analysis Lead, Others: Jo Taylor

Summary of Goals and program design

The goal of this program was to anneal hot pixels and obtain statistics on hot pixels before and after the annealing. The CCD thermoelectric cooler was turned off to allow the detector temperature to rise from about -80 C to the ambient instrument temperature of +5 C. The thermoelectric cooler was turned on 12 hours later and the CCD was cooled to its nominal operating temperature.

Execution

The program executed 1 anneal every 4th week. All 39 parallel orbits were executed successfully.

Summary of Analysis and Results

The anneal results have been posted monthly on the STIS monitors web page at http://www.stsci.edu/hst/stis/calibration/Monitors/anneal . Since the STIS CCD does not have a working temperature control circuit there is no direct measure of the CCD temperature- instead the cooling system is set to a constant current and the data is scaled to a common CCD housing temperature (keyword OCCDHTAV in the first extension [1]) before computing the monitors statistics. Even after scaling the darks to a common temperature the number of hot pixels fluctuates considerably (see Figure 7) meaning that the signature of the temperature fluctuations is not removed entirely. During Cycle 21, the number of post-anneal hot pixels at level 0.1 e-/s varied between 46,563 to 56,840. It was concluded that these fluctuations in the number of hot pixels after each anneal are directly proportional to the CCD housing temperature. Additionally, the median dark current during this cycle varied from 0.01514 counts/pixel/s to 0.0821 counts/pixel/s.

Accuracy Achieved

Due to the fluctuations in the number of hot pixels after the anneals and the variations in the dark current during Cycle 21, it is difficult to derive an accurate measurement for the hot pixel growth rate.

Reference Files Delivered

None

Relevant ISRs

None

Continuation Plans

This program continued in Cycle 22 with PID 13984. No significant changes have been made to the structure of the program for Cycle 22.

Supporting Details

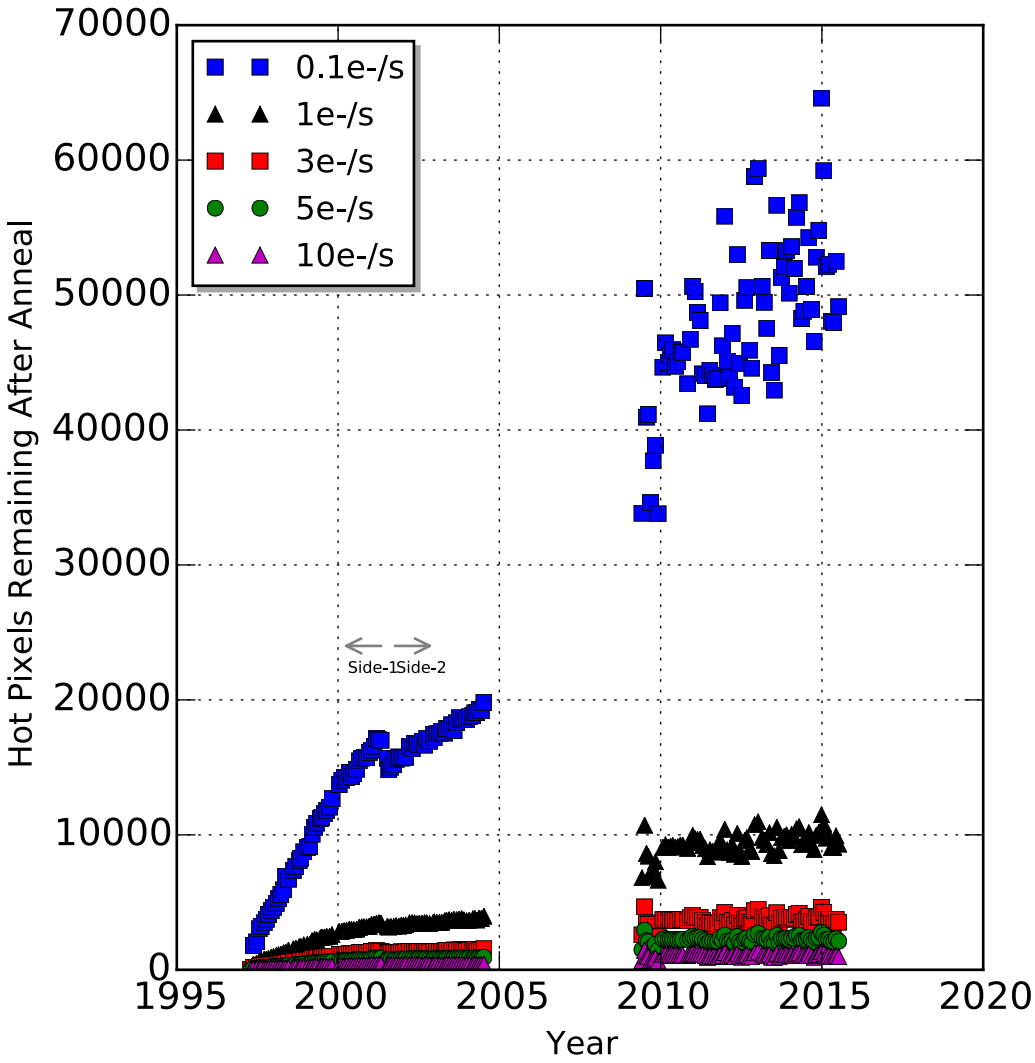

Figure 7. Number of hot pixels for various count rate thresholds remaining after a CCD anneal as a function of time. The scatter in the data is mainly caused by individual pixels being affected by accumulation of radiation damage and CCD temperature fluctuations.

Proposal ID 13538: STIS CCD SPECTROSCOPIC flats

(PI: Hugues Sana)

Analysis Lead, Others: Hugues Sana

Summary of Goals
This program aims to obtain medium resolution (MR) grating flats in order to create the p-flat for CCD spectroscopic observations (which is wavelength and virtually mode independent).

Execution
19 orbits/visits were dedicated to M grating observations. Of these, 10 orbits adopted the G430M/50CCD setup and were spread across the cycle (roughly 1 orbit every ~40 days); while, the remaining 9 orbits used the G430M/52X2 setup positioning the slit at 5 different offset positions in order to make sure that the largest area of the detector was uniformly illuminated.

No failure of any type occurred during the execution of the program, which was completed by August 2014.

Summary of Analysis
The medium resolution (MR) flat exposures were processed separately and independently using an existing python code (See STIS TIR 2013-02 for more details). The code uses CALSTIS to remove bias and darks, as well as to stack (also removing cosmic rays) the frames taken across the cycle with the same setup. The products are then fit column-by-column and row-by-row in order to produce a pixel-to-pixel flat (p-flat) for each setup. These are finally combined in a reference MR p-flat to be used in the data reduction of Cycle 21 science observations. A low-resolution (LR) mode p-flat is created from the MR p-flats by replacing the dust motes with those from an existing LR p-flat (lmode_dustMotes_map.fits)

Accuracy Achieved
The standard deviation of the m-mode and l-mode p-flats is 0.010042 (central 100x100 pixels of the CCD), implying an accuracy of 1% as targeted.

Reference Files Delivered
Further analysis is ongoing to test whether the new Cycle 21 MR p-flat should be delivered.

Relevant ISRs: N/A

Continuation Plans
The program continued in Cycle 22 with only the medium-resolution grating visits. The low-resolution grating visits were dropped as the time evolution of the dust motes is expected to occur on longer time scales.

Supporting Details: N/A

Proposal ID 13539: STIS CCD IMAGING flats

(PI: Hugues Sana)

Analysis Lead, Others: Hugues Sana

Summary of Goals

This program aims at monitoring the stability of the imaging flat field across the cycle as well as the stability from cycle to cycle. The program is identical to the Cycle 20 monitoring program 13136.

Execution

Two sets of STIS CCD imaging flats were obtained 4 times during Cycle 20, within 4 visits, which were scheduled about ~2 months apart from each other. The instrument setup used was MIRVIS/50CCD and MIRVIS/50CORON, standard readout from the D amplifier, and CCDGAIN = 4. No pixel binning or subarray-readouts were used. For each visit, the total integration time for the 50CCD setup was of 3.6 s distributed across 12 exposures. A single 0.3 s exposure per visit was obtained for the 50CORON setup

The STIS CCD imaging flat field data were collected between October 2013 and May 2014 with no failure of any kind.

Summary of Analysis

First, each flat exposure was visually inspected for any macroscopic anomalies. Second, flat frames with the same setup were processed with CALSTIS for bias and dark subtraction and combined to create one coadded, cosmic ray cleaned, super-flat per visit. These were individually analyzed and compared by taking ratios of different pairs to evaluate possible evolution over time. Finally the per-visit super-flats were combined into final cycle super-flats for each set up. For the 50CCD superflat, its low-frequency components is fitted – then removed -- thanks to a spline fitting through the superflat's columns and rows, hence creating a master p-flat for the cycle. The superflats and pflats are compared with similar super-flats and pflats re-computed for previous Cycles.

Table 3 shows the value of the ratios and the standard deviations as measured in the central area of the detector for Visits 2 through 4 super-flats after they have been divided by the Visit 1 super-flat. This shows that there are but only small variation in the level of illumination between the 4 visits.

Table 4 reports the average pixel value and standard deviation as measured in the central part of the detector in the ratios of the Cycle 21 super-flat, compared to the previous cycle super-flats. This table also shows no significant time trends; the two super-flats appear to be stable across (at least 3) cycles. The overall offset between Cy21 and C17 super-flats disappear when removing the low frequency components (i.e. comparing each cycle's pflats instead of the super-flats; see Table 6)

Table 3. Super-flat ratios and standard deviations as measured in the central area of the detector [430:640, 470:565]

Visit Ratio	50CCD	50CORON
2/1	0.9870 ± 0.0022	0.9941 ± 0.0063
3/1	0.9887 ±0.0023	0.9941 ± 0.0064
4/1	0.9919 ± 0.0024	0.9986 ± 0.0064

Table 4. Average pixel value and standard deviation as measured in the central part of the detector ([430:640, 470:565])

Cycle ratio	50CCD super-flat	50CCD p-flat	50CORON superflat
21/20	1.0017 ± 0.0017	1.0001 ± 0.0017	1.0009 ± 0.0035
21/19	1.0051 ± 0.0021	1.0001 ± 0.0011	--
21/18	1.0010 ± 0.0025	1.0000 ± 0.0025	--
21/17	0.9658 ± 0.0028	1.0000 ± 0.0029	--

Accuracy Achieved

We achieved an average count level per pixel (measured in the central detector area, free from defects and dust motes) of ~157000 ADU per visit for the 50CCD "visit super-flats" and 13000 ADU per visit for the CORON super-flats. The average pixel-to-pixel standard deviation within each visit is ~1350 and ~125 for each setup, respectively. The average standard deviation across the 4 visits is 934 and 65 ADU, respectively. This converts to a Poisson noise of 0.25 % and 0.88% per visit, for the 50CCD and 50CORON super-flats respectively; and to an intrinsic pixel-to-pixel standard deviation of 0.86% and 0.96% per visit, respectively.

When the Cycle 21 super-flats are considered the average count level per pixel is ~630000 and ~52100 ADU in the 50CCD and 50CORON super-flat, respectively. The expected Poisson and actual intrinsic noise are 0.13% and 0.85% for the 50CCD, and 0.44% and 0.87% for the 50CORON super-flats. These numbers are identical to those obtained in the previous cycle.

There is an excellent stability in the properties of the Cycle 50 CORON pflats over the last 4 cycles with an average pixel-to-pixel variation rms of 0.12%, i.e. the Poisson noise level.

Reference Files Delivered : N/A

Continuation Plans : No change with respect to the present strategy is foreseen for Cycle 22.

Supporting Details : Table 5 and 6.

Proposal ID 13540: CCD Spectroscopic Dispersion Solution Monitor

(PI: Paule Sonnentrucker)

Analysis Lead, Others: Paule Sonnentrucker

Summary of Goals and program design

Constrain STIS CCD dispersion solution using internal HITM1 wavecal data for all 6 gratings supported for CCD spectroscopic observations. There were no external targets used.

Execution

Yearly program executed on Oct 28, 2013 for a total of 3 orbits, 1 visit each. The data using the G230LB, G230MB, G430L, G430M, G750L and G750M gratings were all successfully taken. The 52x0.1" slit was used in all cases. No data loss occurred.

Summary of Analysis and Results

The HITM1 lamp exposures were reduced with CalSTIS as if they were science exposures. The emission lines in the resulting x1d spectra were to laboratory wavelengths. The comparison between the lamp lines and the laboratory lines was done using three methods:

1. Spk Method: Computes the difference (in pixel) between the laboratory lines and the peak of the observed emission lines in a range of 0.5 pixels around the expected centroid.
2. Gaussian Method: Fits a Gaussian to the observed emission lines and computes the difference between the Gaussian centroid and the laboratory lines
3. WeightSpK Method: Computes the observed emission line centroid weighted mean by using the counts over 2 pixels on each side of the line centroid as weights.

For each method the mean and standard deviation of the differences were calculated and reported below.

Accuracy Achieved

The mean of the difference distribution is lower or equal to 0.1 pixel and the standard deviation is lower than 0.45 pixel in all cases. These results are consistent with those reported for Cy17 by Pascucci et al. (2010; ISR 2011-V1) and Cy20.

Reference Files Delivered

There is no need to deliver a new reference file as the solution accuracy has not changed since Cy17 or since SM4.

Relevant ISRs

These results along with all accompanying figures are included in a multi-cycle ISR (Sonnentrucker P. 2015, in prep).

Continuation Plans

Monitoring program for the CCD dispersion solution was carried over to Cycle 22 with Program 13987 for a total of 3 orbits, 1 visit each, as in Cy21. The gratings and cenwaves used in Cy21 were carried over to the Cy22 monitoring program too.

Supporting Details

Below find, in form of a series of tables and representative figures, the summary of the mean and standard deviations for each grating/cenwave combination derived from the monitoring data analysis.

Table 5. Accuracy achieved for the G230LB and G230MB gratings.

Grating-Cenwave	Mean Offset (pix)	Standard Dev (pix)
G230LB- 2375	0.01	0.28
G230MB- 1713	-0.30	0.31
- 1995	-0.02	0.16
- 2416	0.03	0.22
- 2697	0.13	0.38
- 3115	-0.05	0.10

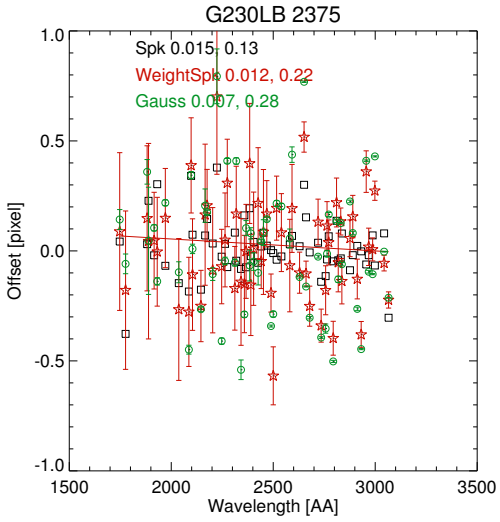

Figure 8. Difference between fitted line centroids and corresponding laboratory wavelengths for all identified lamp lines for the G230LB/2375 setting. The line represents a linear fit to the difference obtained using the WeightSpk method. The mean offset and corresponding standard deviation are listed at the top for each method.

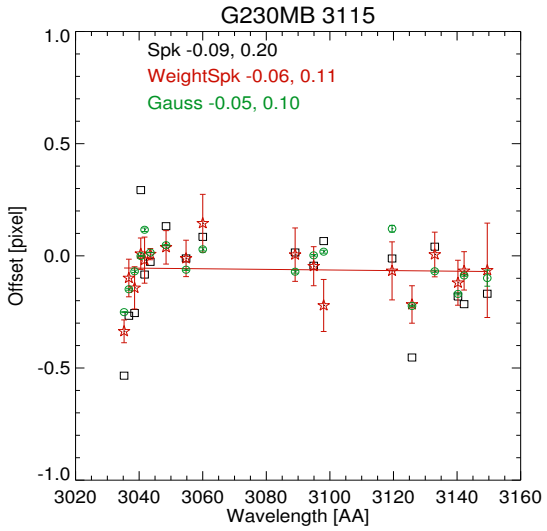

Figure 9. Difference between fitted line centroids and corresponding laboratory wavelengths for all identified lamp lines for the G230MB/3115 setting. The line represents a linear fit to the difference obtained using the WeightSpk method. The mean offset and corresponding standard deviation are listed at the top for each method.

Table 6. Accuracy achieved for the G430L and G430M gratings.

Grating-Cenwave	Mean Offset (pix)	Standard Dev (pix)
G430L- 4300	0.01	0.28
G430M- 3165	-0.02	0.16
- 3680	0.04	0.27
- 4961	-0.05	0.09
- 5471	0.08	0.10

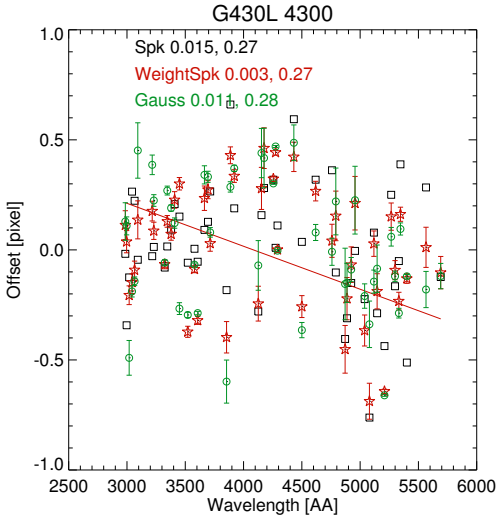

Figure 10. Difference between fitted line centroids and corresponding laboratory wavelengths for all identified lamp lines for the G4300L/4300 setting. The line represents a linear fit to the difference obtained using the WeightSpk method. The mean offset and corresponding standard deviation are listed at the top for each method.

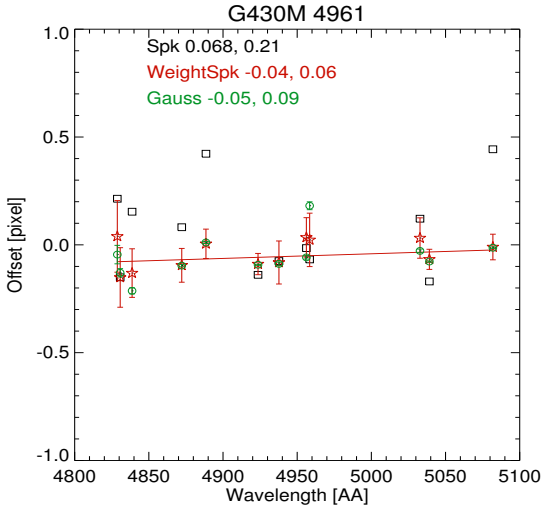

Figure 11. Difference between fitted line centroids and corresponding laboratory wavelengths for all identified lamp lines for the G430M/4961 setting. The line represents a linear fit to the difference obtained using the WeightSpk method. The mean offset and corresponding standard deviation are listed at the top for each method.

Table 7. Accuracy achieved for the G750L and G750M gratings.

Grating-Cenwave	Mean Offset (pix)	Standard Dev (pix)
G750L- 7751	-0.12	0.16
G750M- 5734	0.01	0.13
- 6768	-0.02	0.04
- 8311	-0.02	0.05
- 9336	-0.04	0.07

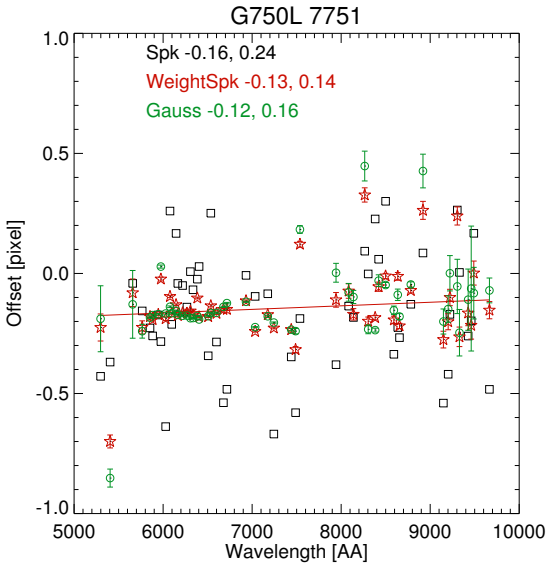

Figure 12. Difference between fitted line centroids and corresponding laboratory wavelengths for all identified lamp lines for the G750L/7751 setting. The line represents a linear fit to the difference obtained using the WeightSpk method. The mean offset and corresponding standard deviation are listed at the top for each method.

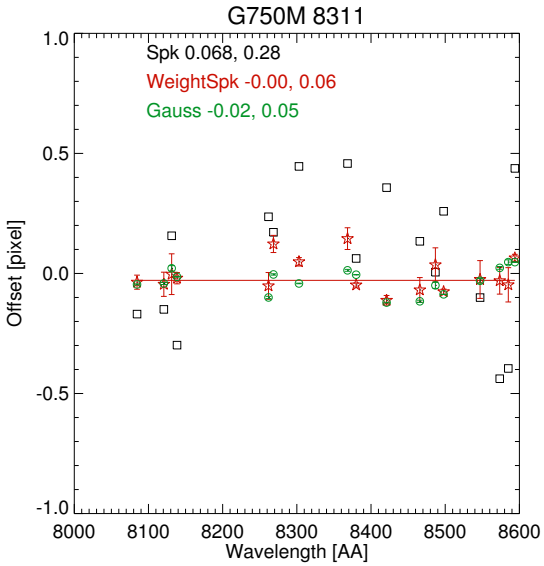

Figure 13. Difference between fitted line centroids and corresponding laboratory wavelengths for all identified lamp lines for the G750M/8311 setting. The line represents a linear fit to the difference obtained using the WeightSpk method. The mean offset and corresponding standard deviation are listed at the top for each method.

Proposal ID 13541: CCD Sparse Field CTE Internal

(PI: Svea Hernandez)

Analysis Lead, Others: Svea Hernandez, Sean Lockwood

Summary of Goals and program design

The purpose of this program is to establish an accurate correction for parallel register CTE losses. Additionally, the program tests the effects of different bias voltages by executing its observations both at GAIN=1 and GAIN=4. Final values for the CTE correction coefficients are then used to update the CCDTAB reference file as needed.

Execution

The program executed successfully as scheduled on November 2013 and December 2012. Visits 01-32 and 65-74 were executed in November, and visits 33-64 and 75-82 executed in December.

Summary of Analysis and Results

Internal calibration lamp observations were taken with narrow slits and used in measuring the sparse field CTE. Slit images are projected at five different positions on the detector and six different flux regimes. Multiple exposures are taken at each position alternating between amplifiers A and C for readout. For each exposure, the average flux per column and centroid of the image profile within a standard 7-row extraction box are estimated. The observed ratio of the fluxes seen by the two amplifiers is fit to a simple model of constant fractional charge loss per pixel transfer. The CTI values are considered to be the fits to the observed flux ratio at a range of source positions along the columns. Due to limited resources, the analysis was restricted to inspection of the individual exposures. It was confirmed that the data were collected nominally. Results of future analysis will be provided at a later time.

Accuracy Achieved

No applicable at the time of publication of this document.

Reference Files Delivered

None.

Relevant ISRs

None.

Continuation Plans

This program was continued in Cycle 22 under PID 13988. The exposures from this program were rearranged in 13988 to acquire ≥ 3 exposures per amplifier, which assists with cosmic ray rejection in the analysis.

Supporting Details

None.

Proposal ID 13542: STIS CCD Full-Field Sensitivity Monitor C21

(PI: Hugues Sana)

Analysis Lead, Others: Julia Roman-Duval

Summary of Goals:

Measure a photometric standard star field in Omega Cen (NGC5139) in 50CCD annually to monitor CCD sensitivity over the whole field of view. This test will give a direct transformation of the 50CCD magnitudes to the Johnson-Cousins system for red sources. These transformations should be accurate to 1%. The stability of these transformations will be measured to the sub-percent level. These observations also provide a check of the astrometric and PSF stability of the instrument over its full field of view.

Execution

Execution occurred as planned between 02-15-2014 and 02-16-2015.

Summary of Analysis

The sensitivity of the STIS CCD is observed to decrease linearly with time, with a rate measured from the STIS sensitivity monitors. The TDS trends are thus obtained from spectroscopic observations, and implemented in CALSTIS for both imaging and spectroscopic STIS CCD observations. The goal of the full-field sensitivity analysis is to verify that the TDS trends derived from spectroscopic observations are applicable to imaging mode.

The star field NGC5139 is observed annually with the 50CCD (clear) filter as part of the STIS full-field sensitivity calibration program. Calibrated and geometrically corrected science files (*sx2.fits) for all STIS CCD full-field sensitivity programs up to C21 were retrieved from MAST. The data set used in this analysis thus includes programs acquired since 2000 up to 2014 (program IDs: 8847, 8912, 9622, 10028, 11854, 12409, 12770, 13139, 13542).

All exposures, obtained with different guide stars, show astrometric offsets of ~1". We first register all exposures with the following method. A reference exposure is chosen, taken as part of program 11854 (obat01050_sx2). The cross-correlation function of the reference exposure and each exposure of the data set is calculated using the IDL routine CORREL_IMAGES, and its maximum located using the IDL routine CORRMAT_ANALYZE. The location of the maximum of the cross-correlation function corresponds to the shift to be applied to the image to match its astrometry to the reference exposure.

Once all exposures are astrometrically registered to the reference exposure, a catalog of stars is identified in the reference exposure using starfinder. The input parameters of starfinder, such as minimum correlation and detection threshold, were empirically determined via a trial-and-error method. We chose a detection threshold of 10 s and a minimum correlation of 0.7. Pairs of stars closer than 0.8" were excluded from the catalog. The starfinder point source extraction algorithm requires a PSF to match the shape of point sources to. We derived the PSF directly in each image using a pre-determined list of stars identified by eye. Each star is centroided and stacked with the IDL routine PSF_EXTRACT in order to estimate the PSF.

Our algorithm then performs aperture photometry for each star in the catalog and each STIS

CCD exposure. First, the background, its standard deviation, and the FWHM of the PSF are estimated in each exposure. Second, an accurate position for each star in the catalog in each exposure is determined. Our registration algorithm is accurate to 1 pixel. Therefore, a test sub-image centered on the position of a star from the catalog, and of width 0.8" is first used to estimate the centroid position of each star in each exposure with sub-pixel accuracy. Once the centroid position is determined, a second sub-image is extracted of size 0.8" and centered on the previously calculated centroid position. Aperture photometry is performed on this sub-image, using an aperture of 5 times the FWHM of the PSF, and annulus also of radius 5 times the FWHM of the PSF, and thickness 5 pixels. The net counts are then converted to magnitudes using the exposure time and the ZMAG keyword populated by CALSTIS, and which includes a correction for the expected TDS trend.

Our algorithm thus provides a catalog of stars and their magnitudes as a function of time, covering the time period 2000-2014. For each star, a linear trend magnitude vs time is fitted (See examples in Figure 1). Figure 2 shows the histogram of the slopes of these trends. The mean slope of the magnitude vs time trend for the STIS CCD detector is 0.41 mmag/year, with a standard deviation of 11.8 mmag/year (based on 108 stars). Over 15 years, this represents a change < 0.6%, lower than the quoted 1 % uncertainty. Figure 3 shows the time dependency of the full-field sensitivity (expressed as a slope in mmag/year) as a function of magnitude.

Accuracy Achieved : 0.6%

Reference Files Delivered: None

Relevant ISRs: ISR 2013-02 (Roman-Duval et al. 2013)

Continuation Plans

Continued in C22. No changes. PID 13989

Supporting Details

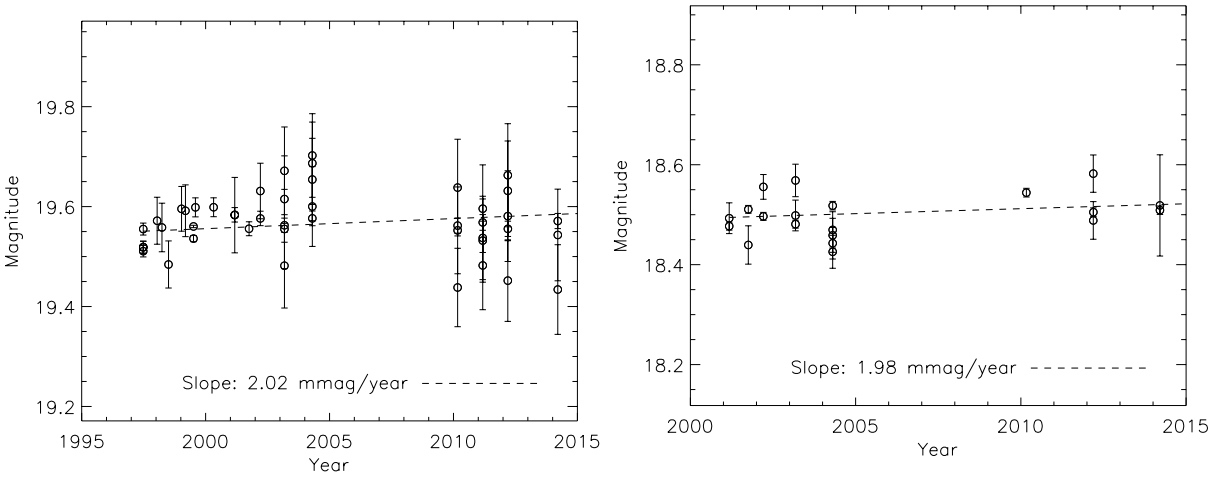

Figure 14. Example of time-dependent full-field sensitivity analysis for a star from the CCD star catalog.

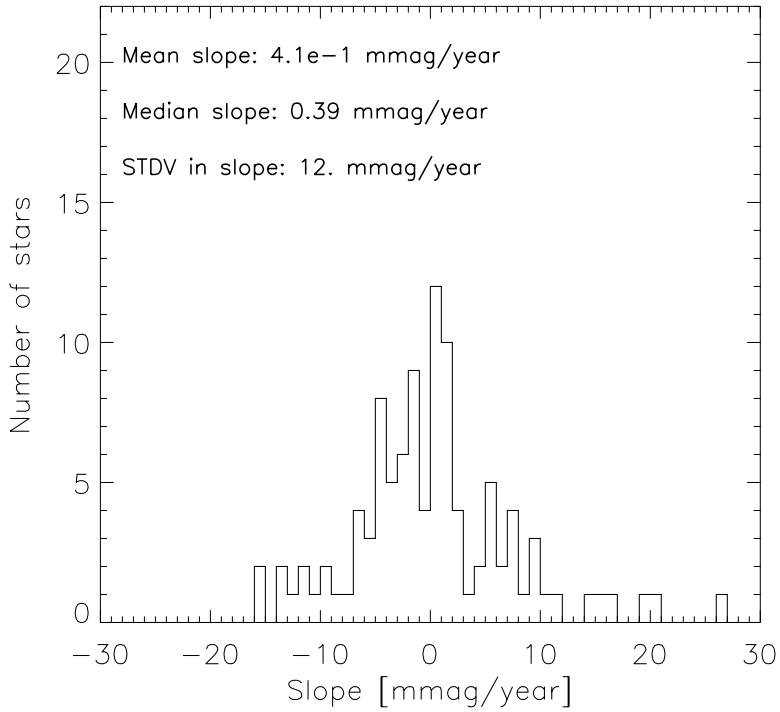

Figure 15. Histogram of the slope of the time dependency of the full-field sensitivity for the STIS CCD.

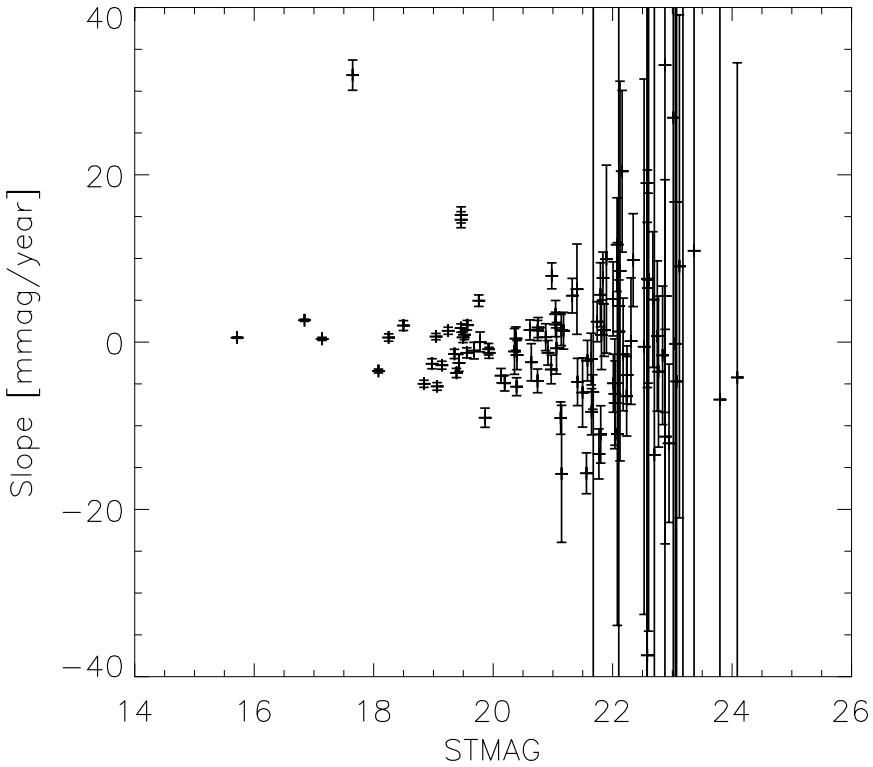

Figure 16. Slope of the full-field sensitivity time dependency as a function of magnitude in the STIS CCD detector.

Proposal ID 13543: Slit Wheel Repeatability

(PI: Audrey DiFelice)

Analysis Lead: Audrey DiFelice

Execution:

Executed nominally on December 2, 2013.

Summary of goals:

Check the repeatability of the STIS slit wheel motion from a sequence of lamp spectra using the grating G230MB (centered at 2697 Å) and the three smallest long slits (52X0.1, 52X0.2, and 52X0.05).

Summary of analysis

A total of 24 exposures were taken over the course of approximately 40 minutes. 9 exposures were taken with the 52X0.1 slit, 8 exposures were taken with the 52X0.2 slit, and 7 exposures were taken with the 52X0.05 slit. The data were processed with the WAVECAL function. The Cycle 21 SHIFTA1 data (the shift in the dispersion direction) seemed to follow the trends of previous cycles. The SHIFTA2 data (the shift in the spatial direction) has not trended strongly over previous cycles, but the Cycle 21 data lies within the bounds of previous cycles. The first data point in each of the three sets was used as a reference point, and all subsequent measurements were zeroed to that reference. The thermal effects of the motion of the slit wheel were then modeled as second order polynomials and subtracted out. After these corrections were applied, the resulting average absolute shift in the dispersion direction (SHIFTA1) was found to be 0.008 pixels, and the resulting average absolute shift in the spatial direction (SHIFTA2) was found to be 0.013 pixels.

Accuracy achieved:

The slit wheel is repeatable to an accuracy of 0.013 pixels.

Continuation plans:

Continue in Cycle 22 as Program 13990.

Proposal ID 13544: STIS/CCD Spectroscopic Sensitivity Monitor for Cycle 21 (PI: Hugues Sana)

Analysis Lead, Others:

Hugues Sana

Summary of Goals and program design

The purpose of Program 13544 is to monitor the spectroscopic sensitivity of the STIS CCDs. This was done using the low-resolution gratings. We observed the white dwarf AGK+81D266 with the instrument configurations listed in Table 8. In brief, Every four months, the L-modes will be observed at settings which cover both the nominal position and the recommended E1 position which places the spectrum closer to the CCD readout. These visits comprise one orbit for each visit. This program also monitors the medium-resolution gratings, with one visit. This visit takes observations at two central wavelength settings of G230MB and G430M, at each of the nominal and E1 pseudo-aperture positions, and at 1 central wavelength setting of G750M (with the addition of an observation at the pseudo-aperature position to that at the nominal position).

We took the ratio of the flux in each spectrum to the flux in a reference spectrum from early in the STIS mission and used these ratios to determine how the STIS CCD sensitivity has changed over time for each spectral element. No ratios were computed in the cases indicated by a reference spectrum of N/A.

There were no changes to this program from Cycle 20

Execution

Observations were taken either once or and three times during the program depending on the mode. The number of observations for each mode is listed in Table 1. For visit L2 (Mar 23, 2015), the FGS could not acquire the guide stars. The acquired data frames were empty. Visit L2 was repeated as visit L4 (HOPR 17, 2015) through HOPR 77602. There were no other missed visits nor any reported observatory or pipeline problems for the remaining visits.

Summary of Analysis and Results

The software described in ISR 2014-02 (Holland et al. 2014) is used to measure the STIS time-dependent sensitivity (TDS). The TDS software works by taking the ratio of the flux in each spectrum to the flux in a reference spectrum from early in the STIS mission. A segmented line is fit to these ratios to determine how the STIS MAMA sensitivity has changed over time for each spectral element. The fitting is blind and does not allow for discontinuities in the TDS. The parameters of the TDS fits are the breakpoint positions and the slopes.

Discrepant data points were observed for G750LB visits L1 (Nov 27, 2013; -1%) and L4 (Apr 16, 2014; -12%). Results from visit L3 (Jul 24, 2014) and subsequent visits in Cycle 22 further confirmed that the problematic data are not representative of the STIS CCD TDS behavior. The jitter plots did not allow us to incriminate an issue with the stability of the pointings and the cause of the issue remains under investigation. Similarly large deviation have been observed in the past and the data were discarded as well. We however kept L1

G750LB data in the analysis (see Figure 19) as it has minimum impact on the quantitative results.

The results for the L modes are presented in Figure 17 to Figure 19. The fitted TDS parameters are summarized in Table 9. The Cycle 21 data show that the weak evidence for a change of slope with breakpoint in June 2012 for the G230LB data was due to statistical fluctuations and all the present trends in all three data sets are fully compatible with pre SM4 trends.

The TDS for the M modes behaves similarly to the corresponding L modes, with the possible exception of G230MB/1995 (Figure 20). More data are however needed to confirm the possible 2010.96 breakpoint.

The 52x2 E1 pseudo apertures were monitored for the first time during Cycle 21, using the same cadence and the same setting as the nominal aperture data. All E1data were compatible with a uniform sensitivity level accross Cycle 21 (see Table 9), with G750L presenting the largest residual. Further data in subsequent cycle may allow to identify a significant trend[1].

Accuracy Achieved

Table 3 gives the root mean square (RMS) values for the best-fit slopes to the TDS for each mode. The overall accuracy in the modelling of the TDS trends is of the order of or better than half a percent per year

Reference Files Delivered:

Synphot files delivered by as part of routine ETC updates.

Relevant ISRs

ISR 2014-02, Holland et al. 2014, The Time-Dependent Sensitivity of the MAMA and CCD Long-Slit Gratings"

Continuation Plans

This program is continued in Cycle 22 under program ID is 13544. There are no changes from program 13991. While the TDS slopes are now well constraints, a quantitative assesment of the quality of the existing TDSTAB reference file should be investigated in a near future.

Supporting Details:

[1] A quick analysis of Cycle 22 G230MB/1955 data (obtained on May 05, 2015) confirms the Cycle 21 results and supports the existence of a 2010.96 breakpoint that marks a slope change from about -0.28 +/- 0.04%/yr to about 0.83 +/- 0.23 %/yr. Impact on the adequacy of current TDSTAB reference file should be investigated in a near future.

Table 8. Observations setup for Program 13544

Spectral Element	Aperture	Wavelength (Å)	Frequncy
G230LB	52X2 / 52x2 E1	2375	3x / yr
G430L	52X2 / 52x2 E1	4300	4x / yr
G750L	52X2 / 52x2 E1	7751	3x / yr
CCDFLAT	0.3X0.09	7751	3x / yr
CCDFLAT	52X0.1	7751	3x / yr
G230MB	52X2 / 52x2 E1	1995	1x / yr
G230MB	52X2 / 52x2 E1	2416	1x / yr
G430M	52X2 / 52x2 E1	3165	1x / yr
G430M	52X2 / 52x2 E1	4194	1x / yr
G750M	52X2 / 52x2 E1	7283	1x / yr
CCDFLAT	0.3X0.09	7283	1x / yr
CCDFLAT	52X0.1	7283	1x / yr

Table 9. STIS TDS parameters for the 3 L-gratings of the CCD monitored by 13544.

Segment	Breakpoint (year)	Slope (%/year)	RMS (%)
Nominal 52x2 aperture			
G230LB			0.22
1	…	+0.77565	
2	1998.96	-1.53719	…
3	2002.92	-0.42579	…
G430L			0.39
1	…	-0.25089	…
G750L			0.27
1	…	-0.15486	…
52x2 E1 pseudo-aperture			
G230 LB	…	0.0000	0.16
G430L			0.39
G750L			0.52

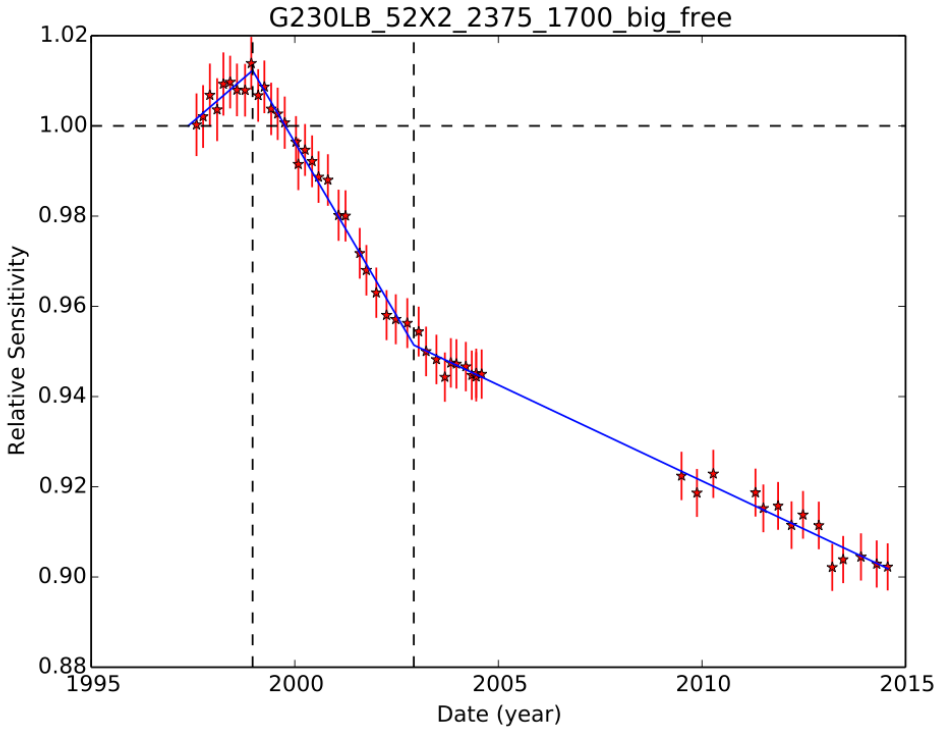

Figure 17. STIS G230LB Time-Dependent Sensitivity. The final three data points are from Program 13544. These points show no indication of a change in the TDS decay since 2002 and confirm that the 2012.5 breakpoint suggested by Cy 20 data were due to random fluctuation

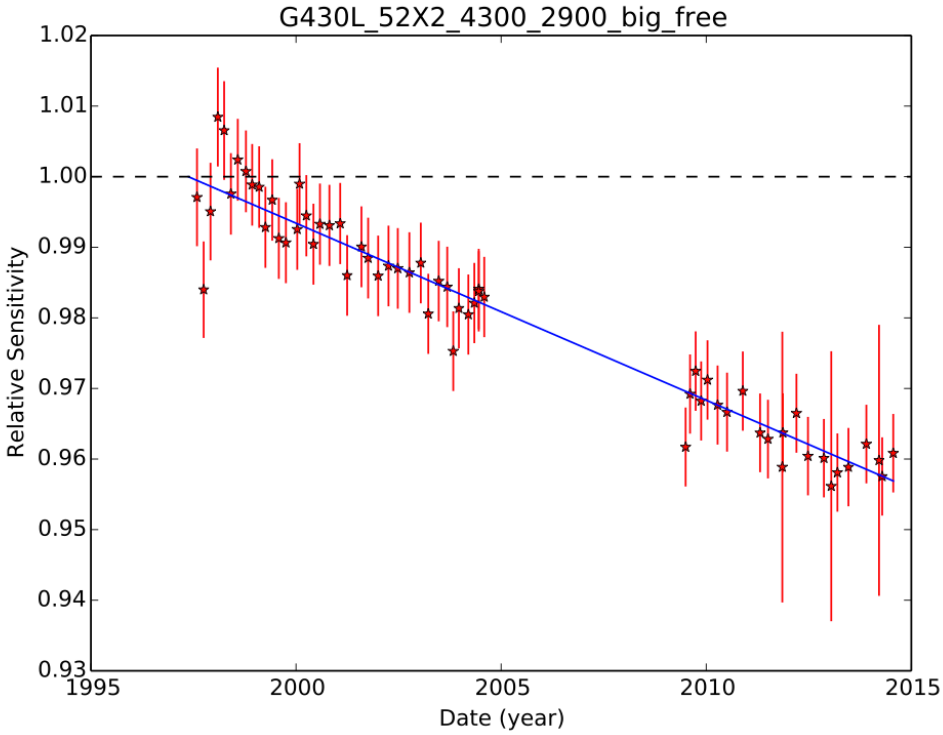

Figure 18. STIS G430L Time-Dependent Sensitivity.

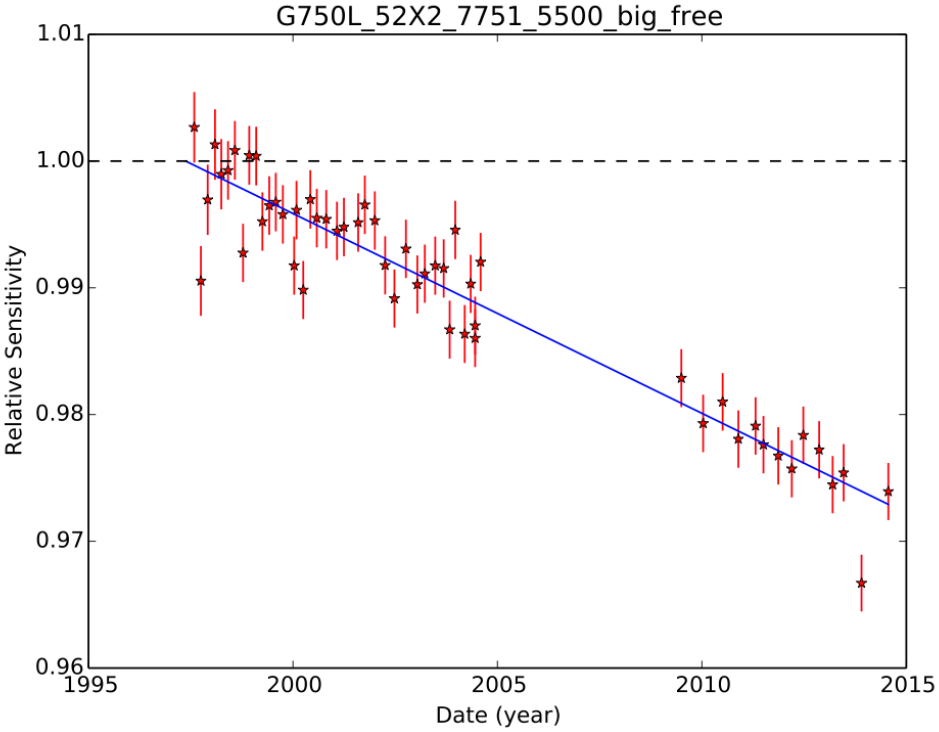

Figure 19. STIS G750L Time-Dependent Sensitivity. The last 2 points are from visits L1 and L3 of the Cy 21 monitoring program.

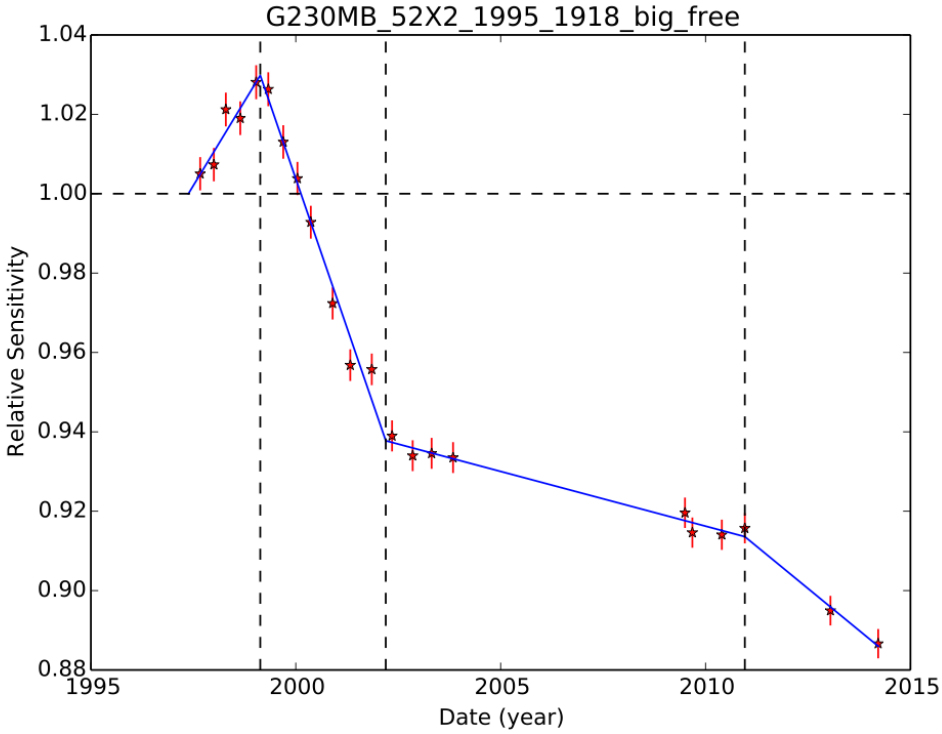

Figure 20. STIS G23MB/1995 Time-Dependent Sensitivity. The last 2 points are from visits M1's in Cy 20 and Cy 21 may indicate a change of slopes from -0.28 +/- 0.03 to -0.85 +/- 0.45 %/yr.

Proposal ID 13546: MAMA Spectroscopic Dispersion Solution
(PI: Paule Sonnentrucker)

Analysis Lead, Others: Paule Sonnentrucker

Summary of Goals and program design
Constrain STIS MAMA dispersion solutions using internal LINE wavecal data for the E140H, E140M, E230H, E230M, G140L, G140M, G130L and G230M gratings, the 0.2x0.09", 0.2x0.06", 0.1x0.09 and 52x0.1 slits and a total of 17 central wavelengths supported for MAMA spectroscopic observations. There were no external targets used.

Execution
This yearly monitoring executed Oct 28, 2013 for a total of 7 orbits, 1 visit each. The data for all grating/cenwave combinations were successfully taken. No data loss occurred.

Summary of Analysis and Results
The LINE lamp exposures were reduced with CalSTIS as if they were science exposures. The emission lines in the resulting x1d spectra were fitted with Gaussian profiles. The emission lines in the resulting x1d spectra were compared to laboratory wavelengths. The comparison between the lamp lines and the laboratory lines was done using two methods:

1. Gaussian Method: Fits a Gaussian to the observed emission lines and computes the difference between the Gaussian centroid and the laboratory lines
2. WeightSpK Method: Computes the observed emission line centroid weighted mean by using the counts over 2 pixels on each side of the line centroid as weights.

For each method the mean and standard deviation of the differences were calculated. The results based on the Gaussian Method are reported below.

Accuracy Achieved
The mean of the difference distribution is lower or equal to 0.2 pixel and the standard deviation is lower than 0.35 pixel in all cases. These results are consistent with those reported for Cy17 by Pascucci et al. (2010; ISR 2011-V1) and Cy20.

Reference Files Delivered
There is no need to deliver a new reference file as the accuracy of the solutions monitored in this program has not changed since Cy17 or since SM4.

Relevant ISRs
These results along with all accompanying figures are included in a multi-cycle ISR (Sonnentrucker P. 2014, in prep).

Continuation Plans
Monitoring program for the MAMA dispersion solutions was carried over to Cycle 22 with Program 13992 for a total of 7 orbits, 1 visit each, as in Cycle 21. The gratings and cenwaves used in Cycle 21 were carried over to the Cycle 22 monitoring program.

Supporting Details
In the following we provide, through a series of tables and representative figures, the summary of the mean and standard deviations for each grating/cenwave combination derived from the monitoring data analysis.

Table 10. Accuracy achieved for the G140 and G230 gratings.

Grating-Cenwave	Mean Offset (pix)	Standard Dev (pix)
G140L - 1425	0.02	0.14
G140M - 1218	0.13	0.14
G140M - 1640	0.03	0.34
G230L - 2376	0.01	0.10
G230M - 1687	0.04	0.19
- 3055	0.15	0.15

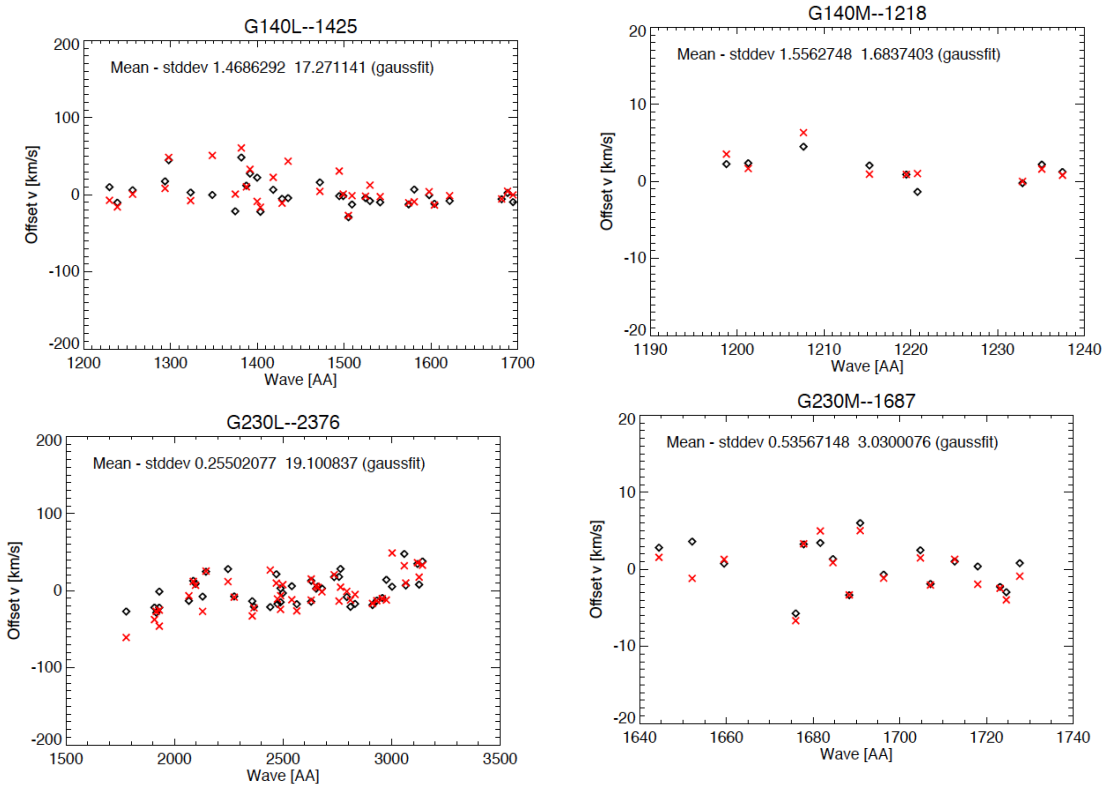

Figure 21. The 4 panels above show the difference between the fitted line centroids and the corresponding laboratory wavelengths for all identified lamp lines. For each setting the mean and standard deviation of the latter differences for the Gaussian fit displayed in velocity space. The black diamonds show results using a Gaussian fit to the lamp emission lines. The red stars show results using a weighted mean centroid fitting. 1 pixel corresponds to 199 km/s for G230L, 16 km/s for G230M, 12 km/s for G140M and 126 km/s for G140L.

Table 11. Accuracy achieved for the E140H and E230H gratings.

Grating-Cenwave	Mean Offset (pix)	Standard Dev (pix)
E140H- 1271	0.05	0.19
- 1343	0.08	0.18
- 1598	-0.01	0.18
E230H- 1763	0.19	0.16
- 1963	0.04	0.25
- 2713	0.09	0.15

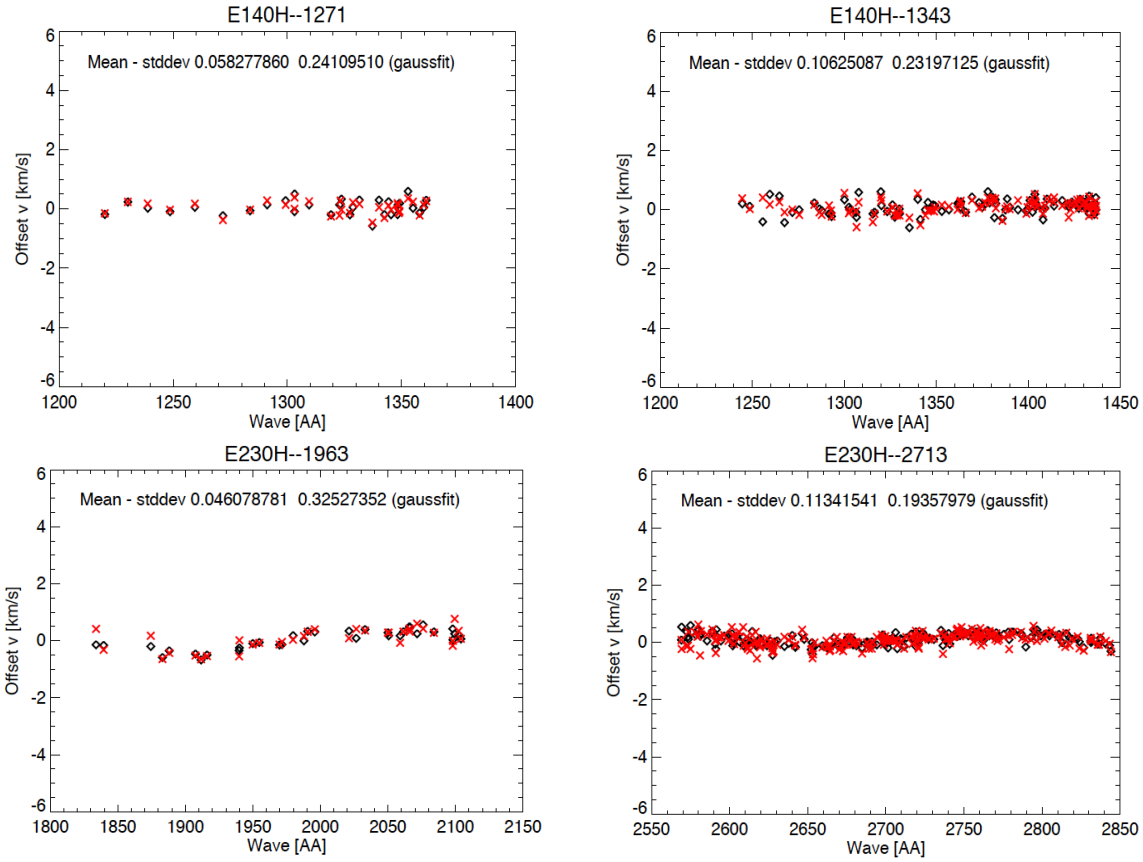

Figure 22. The 4 panels above the difference between the fitted line centroids and the corresponding laboratory wavelengths for all identified lamp lines. For each of the displayed settings the mean and standard deviation of the latter differences were then calculated in velocity space. The black diamonds show results using a Gaussian fit to the lamp emission lines. The red stars show results using a weighted mean centroid fitting. 1 pixel corresponds to 1.3 km/s. The values of mean and standard deviation around the mean obtained from the Gaussian method are reported in the figures in units of km/s.

Table 12. Accuracy achieved for the E140M and E230M gratings.

Grating-Cenwave	Mean Offset (pix)	Standard Dev (pix)
E140M- 1425	-0.06	0.15
E230M- 1978	-0.04	0.19
- 2415	0.01	0.30
- 2561	0.04	0.33
- 2707	-0.02	0.22

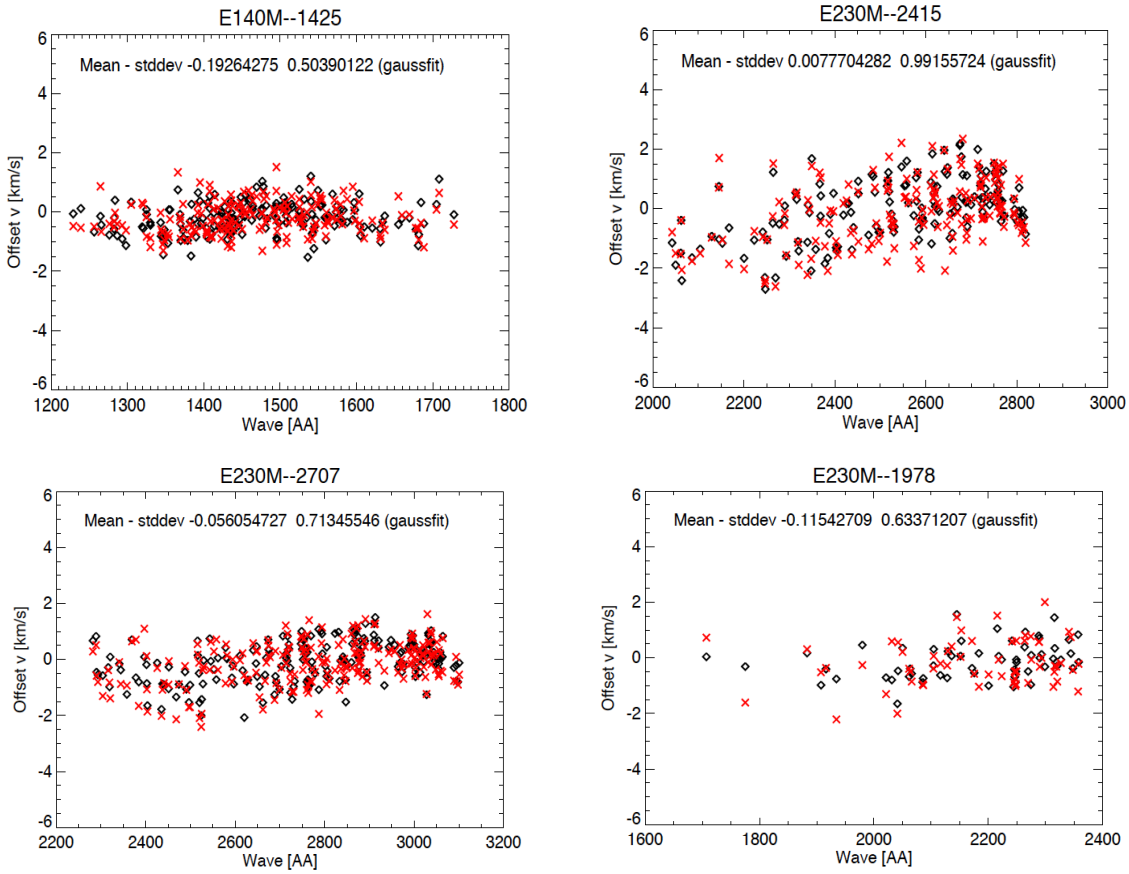

Figure 23. The 4 panels above show the difference between the fitted line centroids and the corresponding laboratory wavelengths was computed for all identified lamp lines. For each setting the mean and standard deviation of the latter differences were then calculated in velocity space. The black diamonds show results using a Gaussian fit to the lamp emission lines. The red stars show results using a weighted mean centroid fitting. 1 pixel corresponds to 3.3 km/s. The mean and standard deviation around the mean using the Gaussian method are reported in the figures in units of km/s.

Proposal ID 13547: STIS MAMA Full-Field Sensitivity Monitor C21

(PI: Hugues Sana)

Analysis Lead, Others: Julia Roman-Duval

Summary of Goals:
The sensitivity of the STIS MAMAs is observed to decrease linearly with time, with a rate measured from the STIS spectroscopic sensitivity monitors. The TDS trends are thus obtained from spectroscopic observations, and implemented in CALSTIS for both imaging and spectroscopic STIS MAMA observations. The goal of the full-field sensitivity calibration program is to verify that the TDS trends derived from spectroscopic observations are indeed applicable to imaging mode, and correcting the decline in sensitivity in imaging mode accurately.

Execution: Execution occurred as planned on 04-10-2014.

Summary of Analysis
The globular cluster NGC6681 is observed annually as part of the STIS full-field sensitivity calibration program. The NUV images are obtained in the F25SRF2, F25QTZ, and F25CN182 filters, while the FUV images make use of the 25MAMA (clear), F25QTZ, and F25SRF2 filters. Calibrated and geometrically corrected science files (*x2d.fits) for all STIS MAMA full-field sensitivity programs up to C21 were retrieved from MAST. The data set used in this analysis thus includes programs acquired since 1997 up to 2014 (program IDs: 7080, 7132, 7720, 7788, 8422, 8425, 8858, 8918, 9623, 10032, 11856, 12413, 12774, 13144, 13547). The NUV and FUV MAMA data are analyzed independently.

All exposures, obtained with different guide stars, show astrometric offsets of ~1". We first register all exposures with the following method. A reference exposure, taken as part of program 11856, is chosen for the NUV (obav01v9q_x2d) and FUV (obav01w4q_x2d). The cross-correlation function of the reference exposure and each exposure of the data set is calculated using the IDL routine CORREL_IMAGES, and its maximum located using the IDL routine CORRMAT_ANALYZE. The location of the maximum of the cross-correlation function corresponds to the shift to be applied to the image to match its astrometry to the reference exposure.

Once all exposures are astrometrically registered to the reference exposure, a catalog of stars is identified in the reference exposure using starfinder. The input parameters of starfinder, such as minimum correlation and detection threshold, were empirically determined via a trial-and-error method. We chose a detection threshold of 10 s and a minimum correlation of 0.7. Pairs of stars closer than 0.4" were excluded from the catalog. The starfinder point source extraction algorithm requires a PSF to match the shape of point sources to. We derived the PSF directly in each image using a pre-determined list of stars identified by eye. Each star is centroided and stacked with the IDL routine PSF_EXTRACT in order to estimate the PSF.

Our algorithm then performs aperture photometry for each star in the catalog and each STIS exposure. First, the background, its standard deviation, and the FWHM of the PSF are estimated in each exposure. The typical FWHM of the PSF is 2 pixels. Second, an accurate position for each star in the catalog in each exposure is determined. Due to geometric distortion effects, stellar positions can vary by up to 10 pixels (particularly in the FUV) between exposures, despite the removal of astrometric offsets. Therefore, a test sub-image centered on the position of a star from the catalog, and of width 0.4" is first used to estimate the centroid position of each star in each

exposure. Once the centroid position is determined, a second sub-image is extracted of size 0.4" and centered on the previously calculated centroid position. This two-step centering procedure allows us to account for all the stellar flux. Aperture photometry is performed on this sub-image, using an aperture of 5 times the FWHM of the PSF, and annulus also of radius 5 times the FWHM of the PSF, and thickness 5 pixels. The net counts are then converted to magnitudes using the exposure time and the ZMAG keyword populated by CALSTIS, and which includes a correction for the expected TDS trend.

Our algorithm thus provides a catalog of stars and their magnitudes as a function of time, covering the time period 1997-2014. For each star, a linear trend magnitude vs time is fitted (Fig. 1). Figure 2 shows the histogram of the slopes of these trends. The mean weighted slope of the magnitude vs time trend for the NUV-MAMA detector is 0.44 mmag/year, with a standard deviation of 4.1 mmag/year (based on 346 stars). Over 15 years, this represents a change of <1%. For the FUV-MAMA, the mean slope is 6.0×10^{-2} mmag/year (based on 46 stars), with a standard deviation of 3.6 mmag/year. This represents a change <1% over 15 years. Figure 3 shows the time dependency of the full-field sensitivity (expressed as a slope in mmag/year) as a function of magnitude.

Accuracy Achieved: FUV-MAMA: <1%; NUV-MAMA: <1%

Reference Files Delivered: None

Relevant ISRs: ISR 2013-02 (Roman-Duval et al. 2013)

Continuation Plans: Continued in C21. No changes. PID 13547

Supporting Details

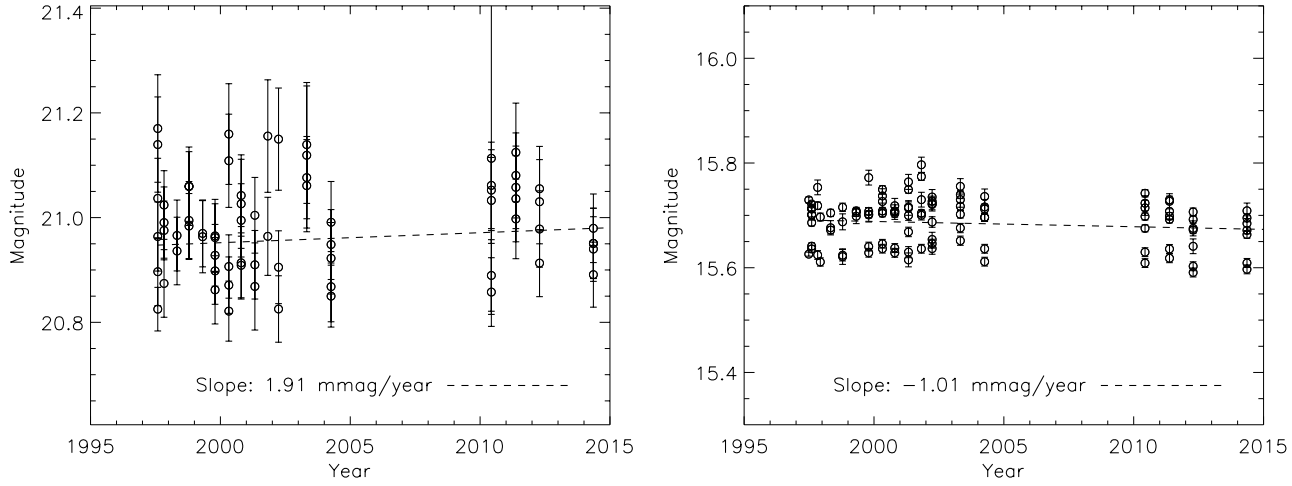

Figure 24. Example of time-dependent full-field sensitivity analysis for a star from the NUV-MAMA star catalog (left) and the FUV-MAMA star catalog (right).

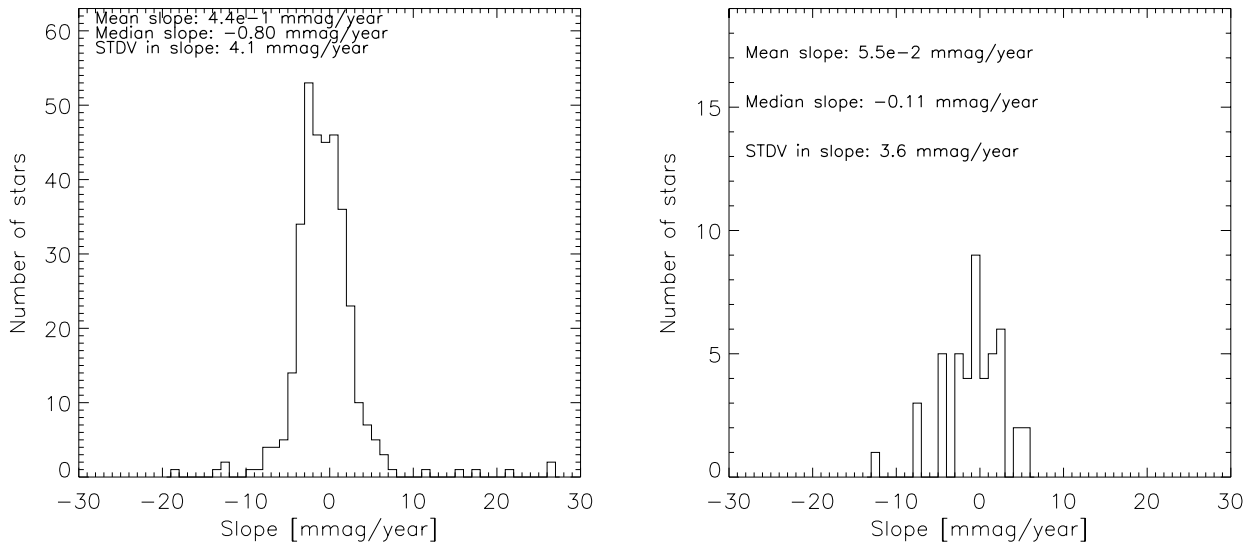

Figure 25. Histogram of the slope of the time dependency of the full-field sensitivity for the NUV-MAMA (left) and FUV-MAMA (right).

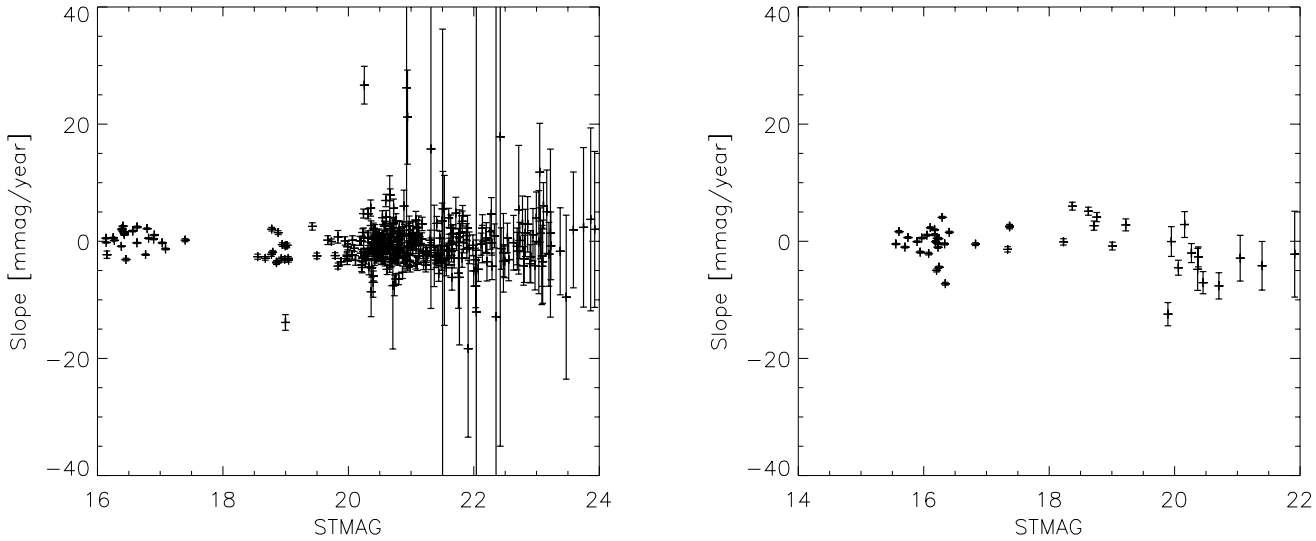

Figure 26. Slope of the full-field sensitivity time dependency as a function of magnitude in the NUV-MAMA (left) and FUV-MAMA (right) detectors.

Proposal 13548 : STIS MAMA Spectroscopic Sensitivity, Focus Monitor, and COS Observations of Geocoronal Lyman Alpha Emission

(PI: Hugues Sana)

Analysis Lead, Others: Hugues Sana, Sean lockwood (see separate summary in COS close-out ISR for the analysis of the COS parallels), Charles Proffitt.

Summary of Goals and program design

The purpose of Program 13548 is to monitor the spectroscopic sensitivity of the STIS MAMAs, monitor the focus, and to characterize Geocoronal Lyman Alpha lines with COS. The MAMAs were monitored using the low and medium resolution gratings, and the echelle gratings. The focus was monitored by measuring the full-width at half-maximum (FWHM) on the target acquisition images. We observed the targets listed in Table 13 with the instrument configurations listed in Table 14.

Execution

Observations were taken several times during the program depending on the mode (see Table 14). Echelle observation E1 (Nov 15, 2013) was affected by GS locking issue and measured relative efficiencies were clearly affected. Visit E1 was repeated as E5 (Jun 12, 2014) approved through HOPR 7641. All other visits were performed as planned.

Summary of Analysis and Results

The software described in ISR 2014-02 (Holland et al. 2014) is used to measure the STIS time-dependent sensitivity (TDS). The TDS software works by taking the ratio of the flux in each spectrum to the flux in a reference spectrum from early in the STIS mission. A segmented line is fit to these ratios to determine how the STIS MAMA sensitivity has changed over time for each spectral element. The fitting is blind and does not allow for discontinuities in the TDS. The parameters of the TDS fits are the breakpoint positions and the slopes.

The results for G140L and G230L are presented in Figure 27 and Figure 28. Table 15 summarizes the breakpoints and slopes (and their errors) for the L modes. The G140L and G230 L data show weak evidence for a change in the rate of sensitivity loss in 2011.2 and 2013.3, respectrively. However, for G140L the scatter in the sensitivity data is larger than the magnitude of the change in the slope while, for G230L, the baseline after the 2013.3 breakpoint is still very limited. In both cases, more data is thus desirable.

The TDS for the M modes qualitatively behaves similarly to the corresponding L modes. Quantitative difference can however be noticed. The G140L/1173 and 1567 settings do not show the same high level of post-SM4 dispersion than the G140L data. The slopes, of the order of -0.40 to -0.45 % / yr are however globally compatible with the G140L ones given the large scatter in the latter data. The fits to both the G140M and G230M data yield slightly better residuals than their low resolution counterpart.

The echelle modes display a larger relative scatter. A 2 breakpoint piece-wise slopes useually reproduces the trends in the data with a root-mean square accuracy of 0.7 to 2%. Manual or automatic cleaning of the deviating point could be implemented to improve the apparence of the results but would not rely on any physical criterion. Compared to previous (post SM4) cycles, most trends seems to sustain themselves. The one exception in the E230M/1978 setting for which most wavelength bins suggest increased slopes after 2013.8. The large scatter in the data and the short baseline however prevent a reliable assesment of the robustness of the suggested break point. Further monitoring is thus needed. Additional discussion on the Echelle TDS behavior can be found in ISR 2014-02 (Holland et al. 2014)

Accuracy Achieved

Table 15 gives the root mean square (RMS) values for the best-fit segmented lines to the TDS data for each L mode. The echelle gratings exhibit systematic deviations up to 3% in their sensitivities from the L-gratings. The scatter is as large as 5% for the echelle gratings. The cause of the large scatter in the echelle modes is under investigation.

Reference Files Delivered

Synphot files delivered by as part of routine ETC updates.

Relevant ISRs

ISR 2014-02, Holland et al. 2014, The Time-Dependent Sensitivity of the MAMA and CCD Long-Slit Gratings"

Continuation Plans

The program was continued in Cycle 21 (PID 13994). There were no major changes.

Supporting Details

Table 13. Targets for each visit.

Visit	Target
L1	GRW+70d5824
L2	GRW+70d5824
L3	GRW+70d5824
M1	AGK+81D266
E1/E5	BD+28D4211
E2	BD+28D4211
E3	BD+28D4211
E4	BD+28D4211

Table 14. Observational setting for Program 13548

Spectral Element	Aperture	Wavelength (Å)	Number (visits)
MIRROR/ACQ	F28X50LP		8
MIRROR/ACQ/PEAK	0.1X0.09		3
MIRROR	F28X50OII		1
G140L	52X2	1425	3
G230L	52X2	2376	3
G140M	52X2	1173	1
G140M	52X2	1567	1
G230M	52X2	2818	1
E140M	0.2X0.2	1425	4
E230M	0.2X0.2	1978	4
E230M	0.2X0.2	2707	4
E140H	0.2X0.2	1416	4
E230H	0.2X0.2	2263	4 (3)

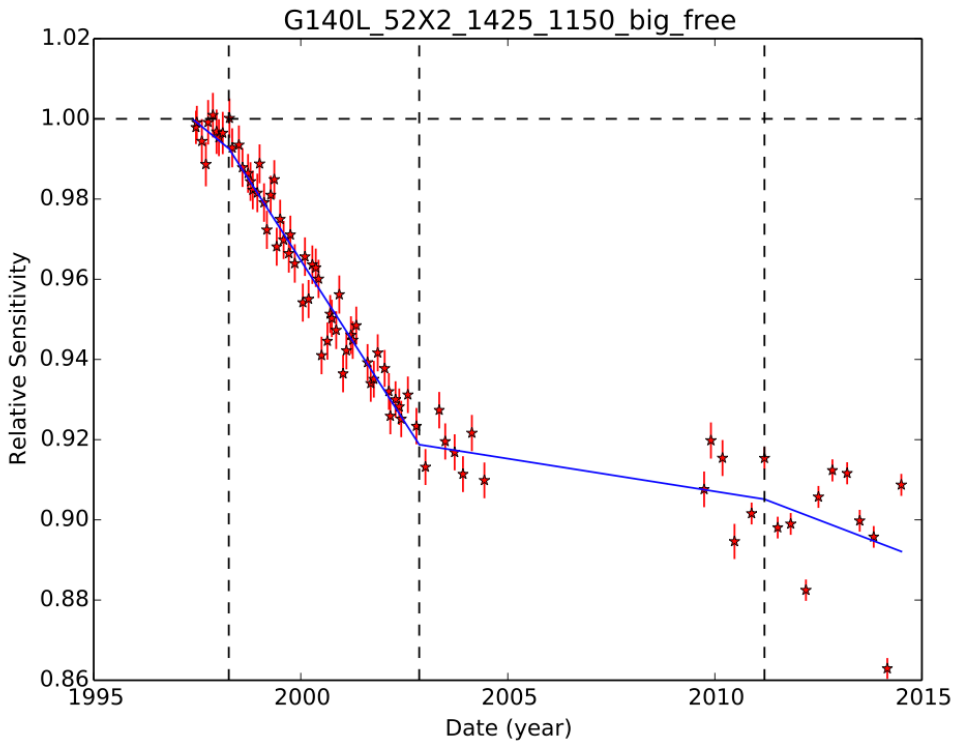

Figure 27. STIS G140L Time-Dependent Sensitivity. The final three data points are from Program 13548 and are indicative of a large scatter. It is unclear whether the 2011.2 breakpoint is significant or induced by systematics in the data (e.g. affecting the 2014.2 point).

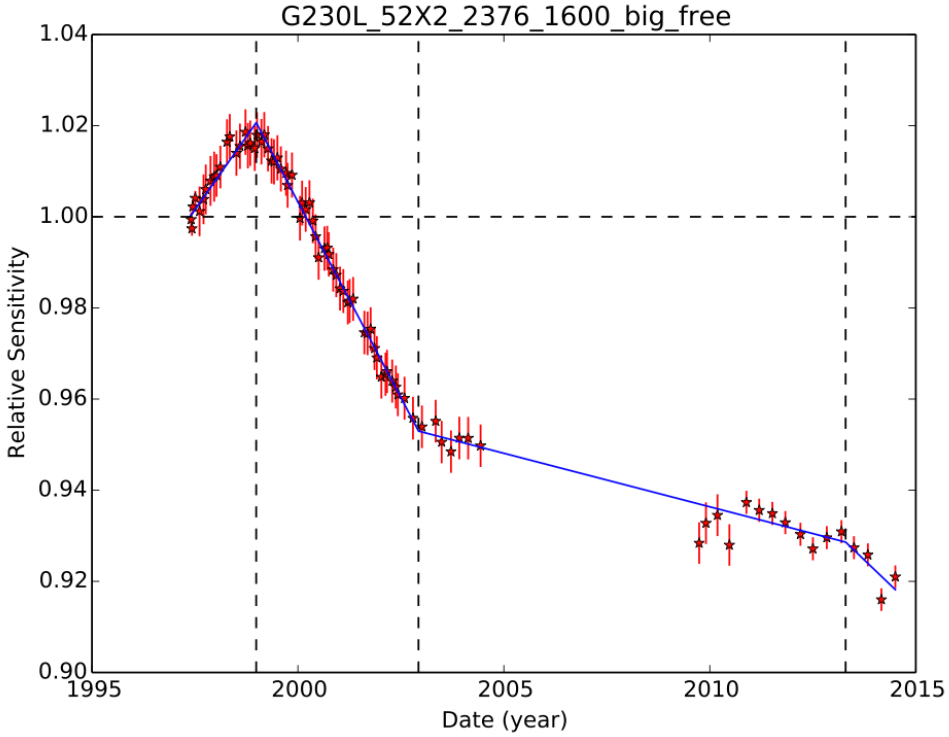

Figure 28. STIS G230L Time-Dependent Sensitivity. The final three data points are from Program 13548 and may suggest a slightly enhanced slope.

Table 15. STIS Time-dependent sensitivity parameters obtained from the TDS fit for the L gratings

Segment	Breakpoint (year)	Slope (%/year)	RMS (%)
G140L			0.726
1	…	-0.837 +/- 0.715	
2	1998.26 +/- 0.55	-1.696 +/- 0.53	…
3	2002.86 +/- 0.17	-0.163 +/- 0.033	…
4	2011.20 +/- 1.07	-0.394 +/- 0.089	…
G230L			0.241
1	…	+1.285 +/- 0.155	…
2	1998.99 +/- 0.09	-1.717 +/- 0.069	…
3	2002.93 +/- 0.17	-0.235 +/- 0.023	…
4	2013.30 +/- 0.46	-0.865 +/- 0.336	

Proposal ID 13549: FUV MAMA Dark Monitor

(PI: Colin Cox)

Analysis Lead, Others: Colin Cox

Summary of Goals and program design
Goal is to characterize the dark rate of the FUV MAMA to assist in scientific data processing and to highlight any irregular performance of the detector.
The monitor takes six 1300 second TIME-TAG darks every six weeks. The exposures are distributed over about six hours from initial turn-on to characterize the rate increase as a function of turn-on time and temperature.

Execution
All visits completed as scheduled.

Summary of Analysis and Results
The schedule was changed in the previous cycle and continued in the current cycle to allow for a sequence of six measurements at each visit. This is to characterize the dark rate as a function of time turned on and temperature. This was successful and showed that the dark rate can be reasonably characterized as a quadratic function of temperature. This provides the observer with a much better estimate of the dark rate in a particular observation than can a single number. The dark rate shows no long term change as illustrated in the supporting details and remains at approximately 10^{-4} counts per pixel per second..

Accuracy Achieved
Since each dark image contains about 200000 counts, the statistical accuracy of the mean count rate is 0.2 %

Reference Files Delivered

FUV monitor web page was regularly updated. While no formal calibration files are supplied this does include a table of all measurements.

Relevant ISRs

The ISR " Dark count rates in the STIS FUV MAMA" has been submitted and reviewed. Awaiting final review and publication.

Continuation Plans

The program is continued in Cycle 22 as proposal 13995 with no changes.

Supporting Details

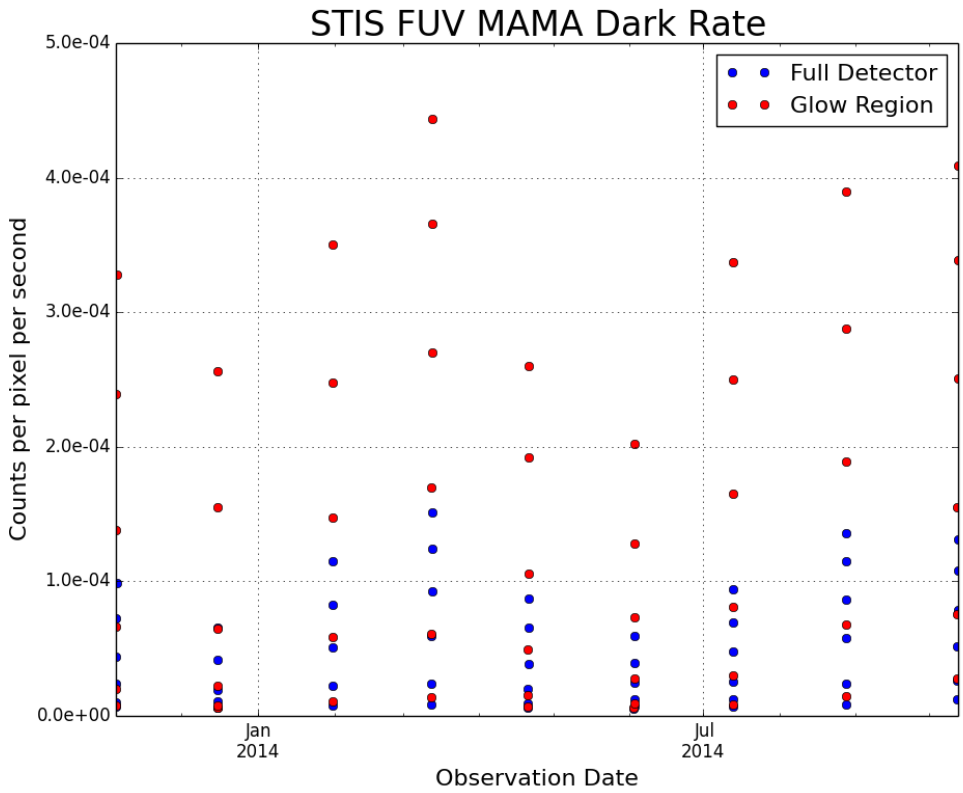

Figure 29 shows the measured count rates during this cycle. Red circles indicate the count rate in an area which shows higher than average rates. No long term trend is indicated.

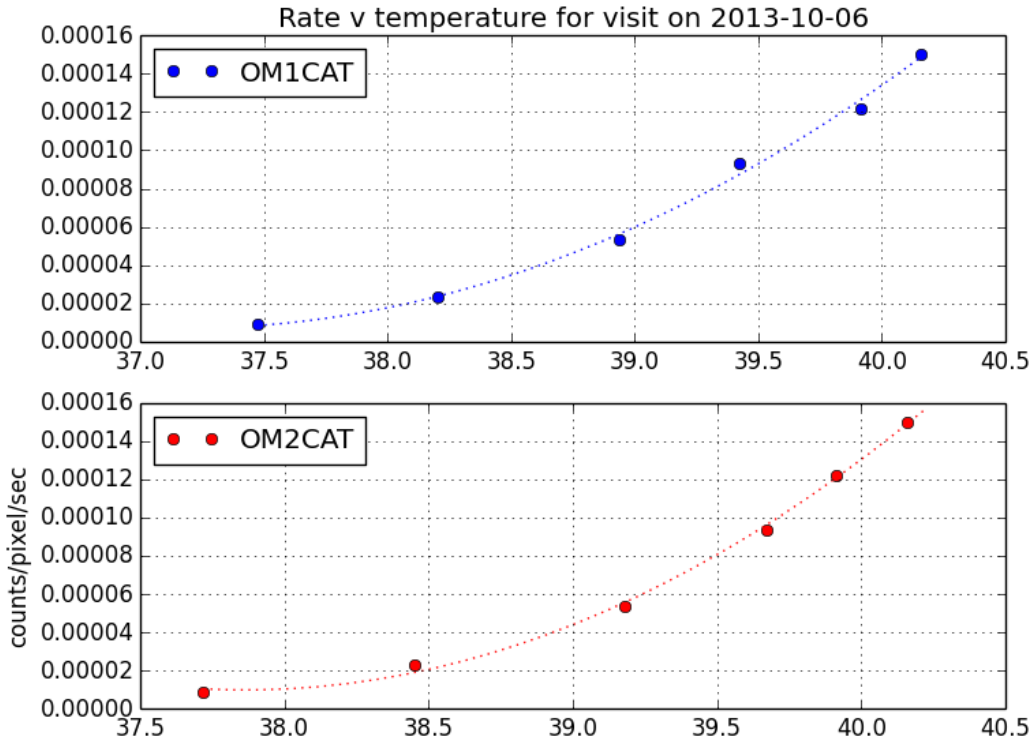

Figure 30 illustrates the dependency of dark rate on two measured temperatures OM1CAT and OM2CAT. As for the NUV MAMA, a quadratic form provides a good model.

Proposal 13550: NUV MAMA Dark Monitor

(PI: Colin Cox)

Analysis Lead, Others: Colin Cox

Summary of Goals and program design

The aim of the program is to characterize the dark rate in the NUV MAMA, partly for analysis support and also to highlight any changes in the instrument behavior. The dark rate is so low that it is rare to use it to subtract from measured images.

The basic monitor takes two 1300s TIME-TAG darks bi-weekly. The pairs of exposures are linked so that they are taken about 6 hours apart in the same SAA free interval. This pairing of exposures makes it easier to separate long and short-term temporal variability from temperature dependent changes.

Execution

All visits were completed as scheduled.

Summary of Analysis and Results
Analysis was continued as reported in ISR 2013-01, "Dark count rates in the STIS MAMA". The slow exponential decline in count rate was maintained with a current value near 1.5×10^{-3} counts per pixel per second.

Accuracy Achieved
The mean rate is typically based on about 2.2×10^{6} counts thereby providing an accuracy of about 0.07%

Reference Files Delivered
Monitoring web page maintained. This gives plots and full history of results since SM4

Relevant ISRs

Continuation Plans
Program continuing unchanged in Cycle 22 as proposal 13996

Supporting Details

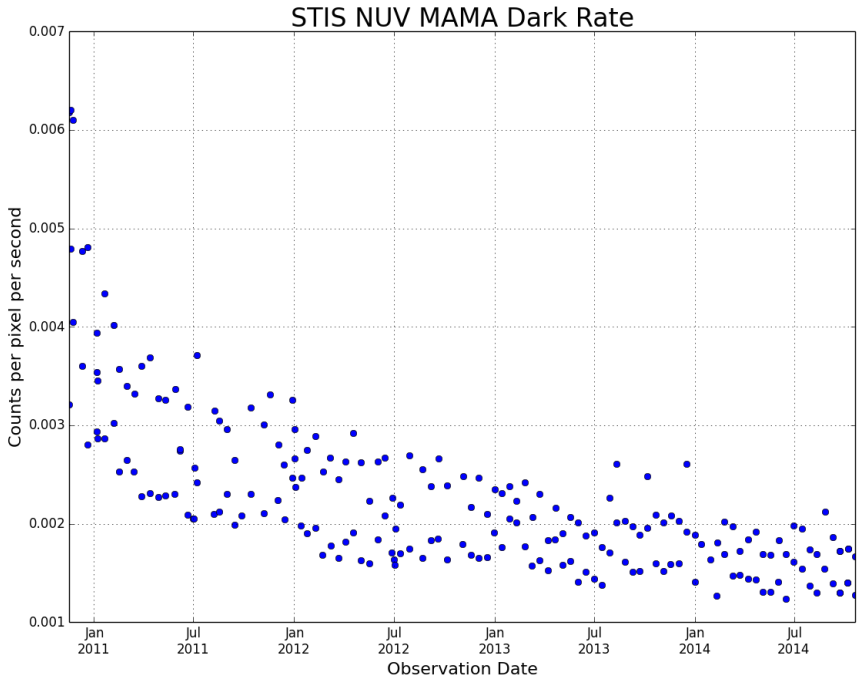

Figure 31. Copy of the figure supplied to the monitoring web page.

Proposal ID 13551: STIS MAMA NUV Flats

(PI: Hugues Sana)

Analysis Lead, Others: Hugues Sana

Summary of Goals
This program is aimed at obtaining NUV-MAMA flat-field observations for the construction of pixel-to-pixel flats (P-flats) with a SNR of ~100 per binned pixel. The flats are obtained with the DEUTERIUM lamp and the medium-resolution grating G230M. The choice of central wavelength and slit combination depends on the observed count level within each exposure.

STIS NUV-MAMA flats are taken every other cycles (i.e. during odd number cycles) in order to preserve the remaining DEUTERIUM lamp lifetime. In addition they are taken mainly for monitoring purposes, as there is a limit to how well one can correct the MAMA data.

Execution
We used a total of 11 orbits to collect the desired signal. These were executed in the period December 2013 – April 2014 making sure that the visits were not consecutive in order to limit the lamp usage in the case of a technical failure (e.g. a detector safing without an instrument suspend could prevent data from being collected even though the lamp would still be turned on). The instrument setup adopted during the entire program was the same used in the last exposure of the previous NUV-MAMA monitoring program, i.e. G230M/2419/52X0.5 with exposure time equal to 3588 s. In addition five different SLIT-STEP positions were adopted during the program execution in order to uniformly illuminate the whole detector.

All the visits where completed successfully with no failure of any type.

Summary of Analysis
The frames collected within the program were combined and processed using the existing IDL code by Brown et al. (2002, STIS-TIR 2002-03). They were also combined and processed using a PI written script which creates the P-flat by column-by-column and line-by-line fitting of the cumulative data signal with a high (~7-9) order polynomial. The comparison of the two methods has been discussed in the STIS-TIR 2013-01. For flat-field correction of science data only a combination of P-flats obtained with Brown's IDL code should be used.

P-flats were created for Cycles 11, 17, 19 and 21 and compared in order to evaluate possible changes in the detector characteristics. Changes in the pixel-to-pixel response are more difficult to assess as this should be done using higher SNR data (~100 per high resolution un-binned element, in place of the current SNR~50) and with the same instrument setup. Each STIS NUV MAMA flat monitoring programs adopted different instrument setups (Figure 32) in order to maximize the incoming photon flux and lamp lifetime and did not collect sufficient signal to directly test the pixel-to-pixel response.

The P-flat produced within this program is not suitable – alone – as reference file for flat-fielding of science observations. Following Brown et al. (2002) analysis the P-flat from at least 5 different cycles should be combined in a master reference P-flat. We have verified that using the individual P-flats from Cycles 21, 19, 17 and 11, as well as a master P-flat combining all these cylcles, the

science reduced data do not reach the same SNR as when flat-fielded with the reference P-flat currently in use (mbj1658do_pfl.fits, produced in 2002), even outside the part of the spectrum affected by residual lamp/slit features (Figure 33 and Figure 34). P-flat obtained with the G230M/2338 setup indeed present a residual features produced by the non perfect removal of the emission lines and/or by imperfections of the slit edges in combination with the slit reproducibility precision.

Ratioed images of the P-flats from cycles 11, 17, 19 and 21, and of the Cycle 1 to 21 master P-flat were also computed to search for possible detector changes. Table 16 provides the standard deviation (rms) of the ratioed images, measured in the area [300:600,600:800] (i.e., free from residual feature). As noticed in the Cycle 19, the residuals increase with time and are larger when the Cycle 21 P-flat is compared with the P-flat currently in use (see Table 24 below). We also visually inspected the ratioed images (see Figure 34). We conclude that the increased residual most likely results from two effects:

- a change in the fixed pattern component of the P-flat (see Figure 34), with a peak to peak relative variation of up to 20% (Figure 35)
- a change in the relative amplitude level of the odd-even effect of the order of 2 to 3% (Figure 35 and Figure 36).

While the impact of the change in the fixed pattern component on the actual science observation is likely limited (see also discussion in Cycle 20 ISR), it may be possible be possible to produce a new reference P-flat once STIS NUV MAMA flats monitoring programs of 23 has been completed and the residual P-flat line/slit signature is corrected or masked. However, careful comparison with the reference P-flat currently in use should be performed before its replacement. In addition, it is known (Brown et al. 2002) that there is a limit to how well one can correct the MAMA data.

Accuracy Achieved

The total collected signal during the cycle 21 STIS NUV MAMA flat monitoring delivers the average of 2115 counts per un-binned/high resolution pixel. This corresponds to a SNR of 50 and 100 (assuming Poisson distribution) per high and low (2x2 binning) resolution element respectively and matches the program requirements.

The Cycle 21 P-flat obtained following Brown prescription has an average value per high resolution element (un-binned pixels) of 0.9998 with standard deviation of 0.5735. This, by no means should be considered as the accuracy obtained by this program as the STIS MAMA flat pixel value distribution is bi-modal (odd-even column effect) and the measured standard deviation reflects such bi-modality. Once the odd-even effect is taken into account (statistics performed on images formed by only a combination of odd/even rows and columns), the rms drops in the range 0.08-0.17.

The rms of each individual pixel computed across the Cycle 17, 19 and 21 individual P-flats (corrected for the small sample size) has an average value of about 0.02. This is compatible with the estimated Poisson noise as well as with the rms of the ratio of individual Cycle 17, 19 and 21 P-flats to that of the master P-flat (encompassing data from Cycles 11 to 21; see Table 16). This value can thus be considered as the average precision of the program. The 1-sigma dispersion on this average precision is of a factor of 2.

Reference Files Delivered

N/A

Relevant ISRs: STIS TIR 2013-01.

Continuation Plans

The STIS NUV MAMA flat monitoring program should continue in Cycle 23 with no significant changes other than a possible instrument setup "adjustment", to allow the collection of the required SNR.

Supporting Details

Table 16. The standard deviation (rms) of the ratio images. The odd columns indicates the cycles which P-flats are being ratioed. The even columns reports the rms, measured in the area [300:600,600:800] (free from "spurious" features, see text).

P-flat ratio (Cycles)	Residual RMS	Ratio with New master (11+17+19+21)	Residual RMS	Ratio with mbj1658do	Residual RMS
11/17	0.040	11/master	0.028	11/mbj	0.032
11/19	0.044	17/master	0.020	17/mbj	0.047
11/21	0.042	19/master	0.022	19/mbj	0.053
17/19	0.033	21/master	0.023	21/mbj	0.050
17/21	0.034				
19/21	0.035				

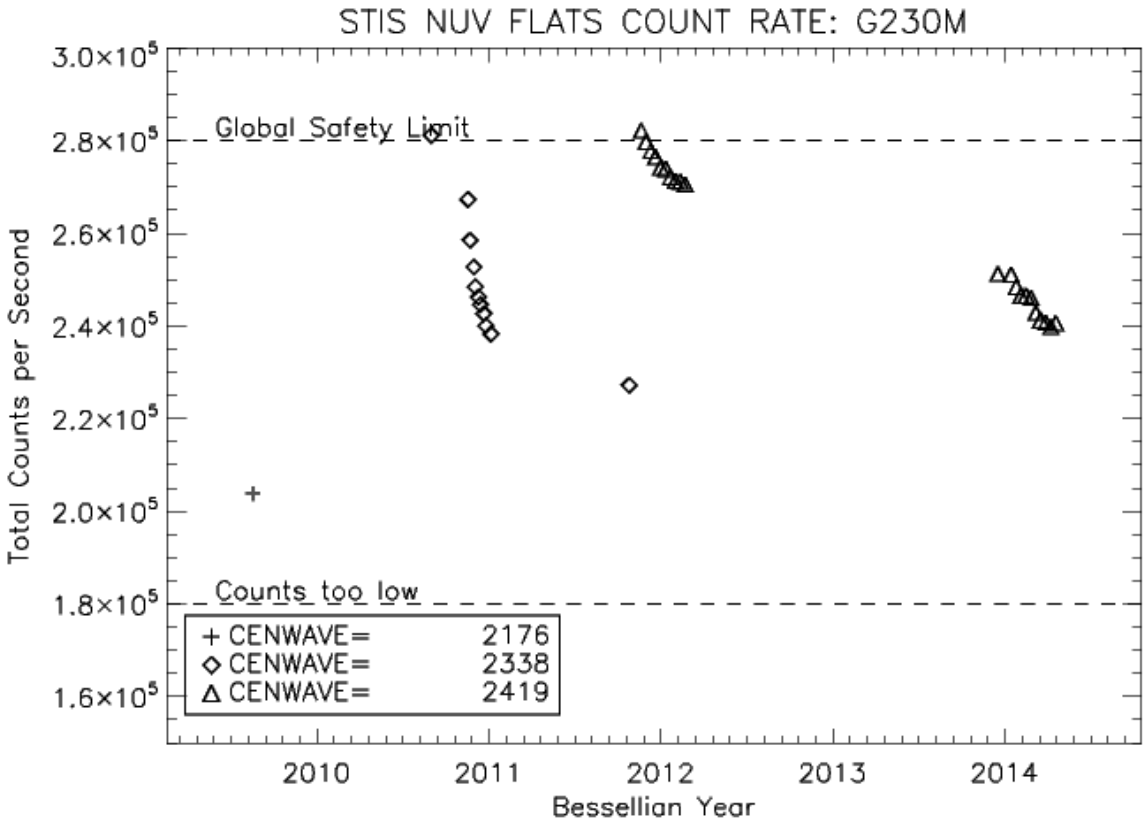

Figure 32. Evolution of the countrate of the STIS NUV flat observations since SMOV4

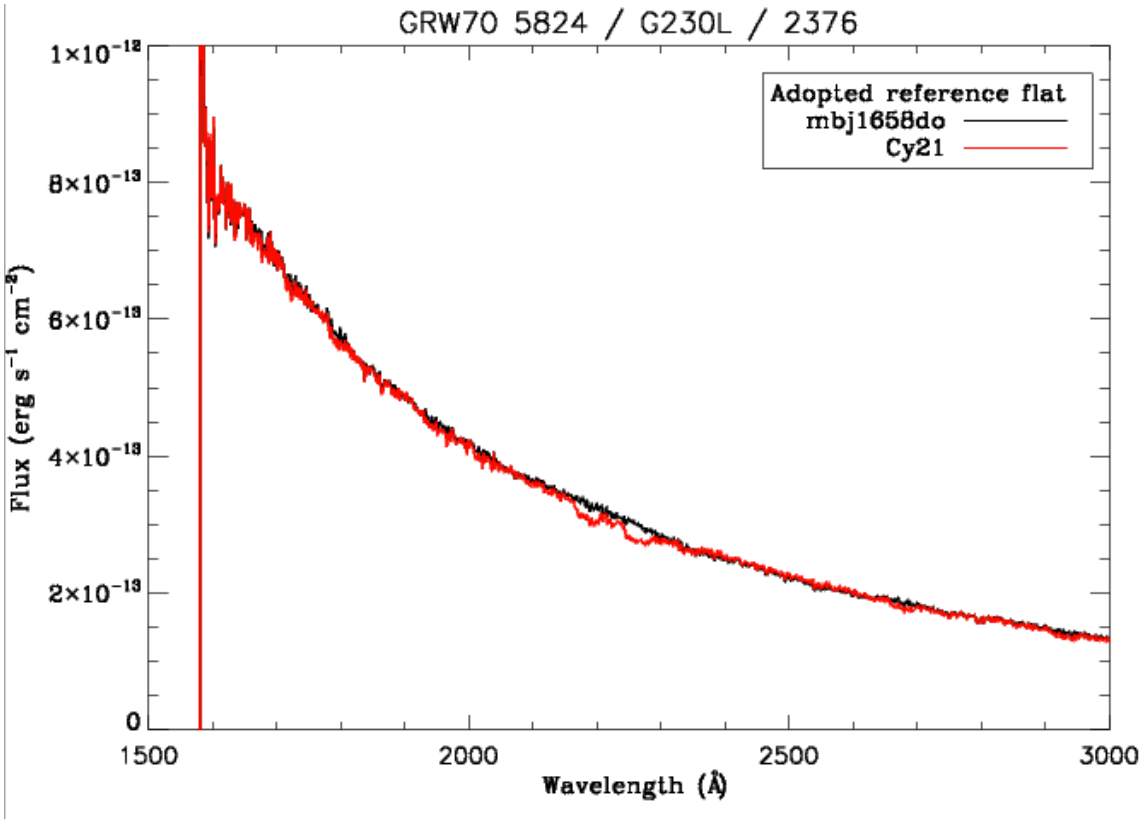

Figure 33. G230L/2376 observations of the stanrard star GRW 70D5824 reduced with two different reference P-flats (see legend). Artifacts arounds 2200 Angstroms are present when using the Cycle 21 P-flat.

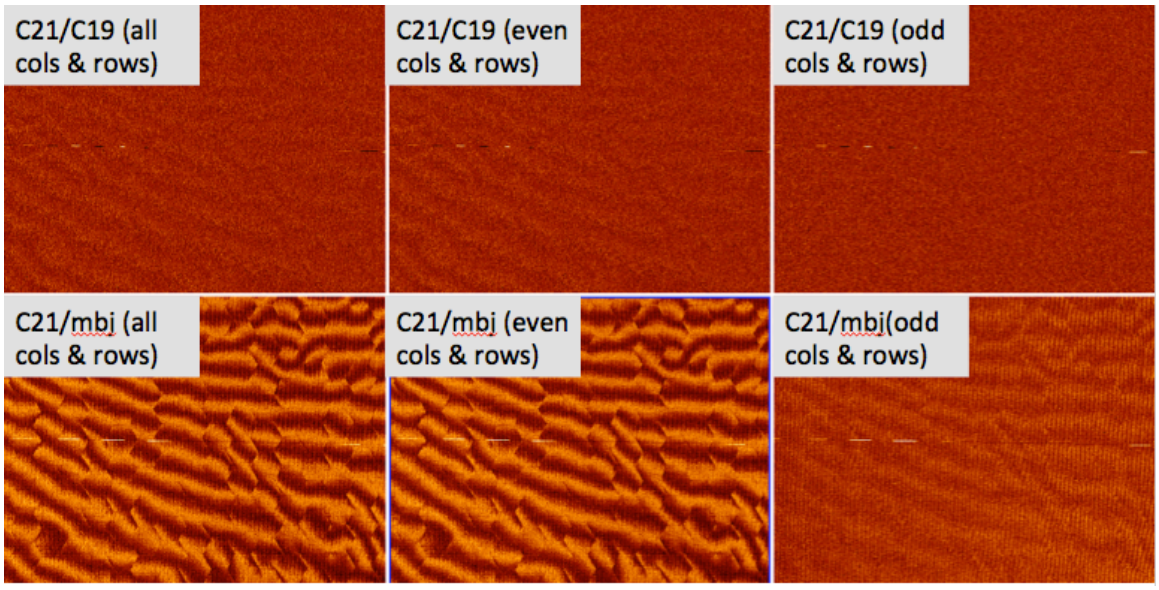

Figure 34: Ratio of Cycle 21 to 19 P-flats (top row) and of Cycle 21 to mbj1558do P-flats (bottom row). The 1st column provide the entire image while Cols. 2 and 3 provide images built with only the even or odd columns and rows of the detector. The color scale used is linear and extends between 0.6 and 1.7.

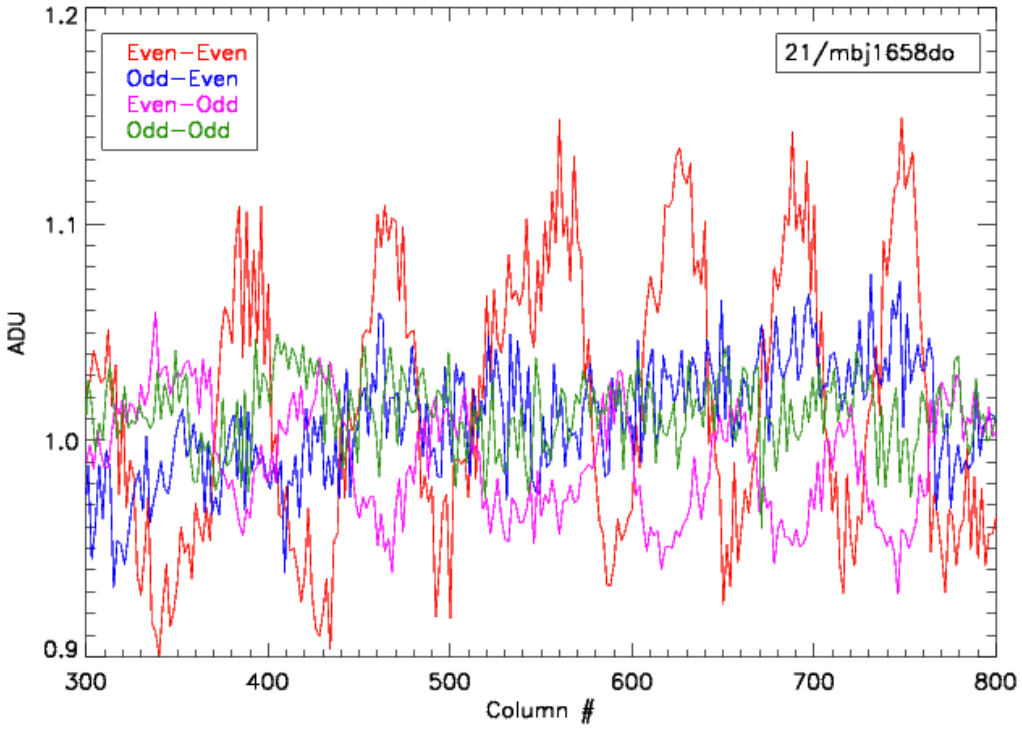

Figure 35: Slice in the ratio image of Cycle 21 to mbj1658do P-flats for different combination or rows and columns

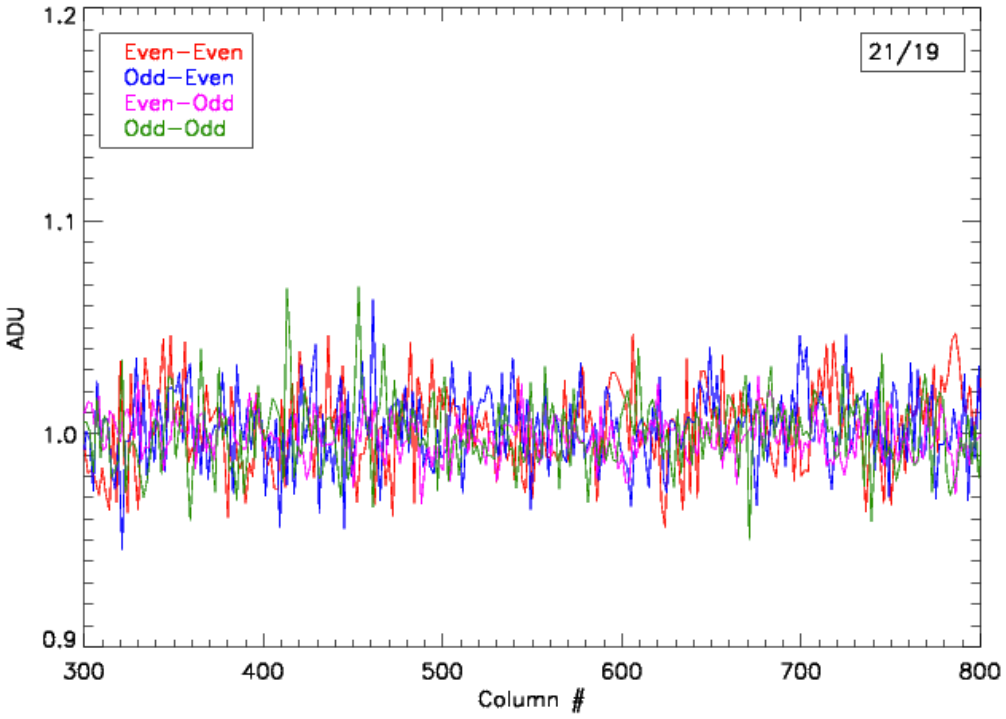

Figure 36: Slice in the ratio image of Cycle 21 to Cy 19 P-flats for different combination or rows and columns.

Proposal ID 13552: STIS MAMA Fold Distribution

(PI: Thomas Wheeler)

Analysis Lead, Others: Thomas Wheeler, Alan D. Welty (CoI)

Summary of Goals
The performance of MAMA microchannel plates can be monitored using a MAMA fold analysis procedure that provides a measurement of the distribution of charge cloud sizes incident upon the anode giving some measure of change in the pulse-height distribution of the MCP and, therefore, MCP gain. The goal is to continue monitoring the two STIS MAMA detectors and comparing the results with previous test results to detect trends or anomalous behavior. This proposal is based on Cycle 20 Proposal 13149.

Execution
This proposal successfully executed on May 1-2, 2014.

Summary of Analysis
The engineering telemetry data was examined (voltages, currents, temperatures, relay positions, and status) for agreement with predicted values and previous ground and on-orbit test data. The MAMA engineering telemetry event counter was used construct a histogram of the number of counts for each fold. The results for each detector are compared and combined with previous test results. Posttest, a dark exposure was taken where the counters were cycled and were plotted in a histogram and compared with earlier results.

No anomalous behavior was detected for either MAMA. The NUV MAMA does exhibit a known high dark count rate caused by widow phosphorescence that has been decreasing since SMOV4. Results are sent to the COS/STIS Science Team and V. Argabright of Ball Aerospace for review and comments.

Accuracy Achieved
Position of the peak in the fold distribution can be measured to about 5% accuracy from this procedure.

Reference Files Delivered
N/A

Relevant ISRs
No ISRs will be published.

Continuation Plans
This monitoring program will continue in Cycle 22 Proposal 13998. No modifications are expected.

Supporting Details

Below are the FUV fold histogram and the post-test dark count histogram followed by the NUV fold histogram and the post-test dark count histogram.

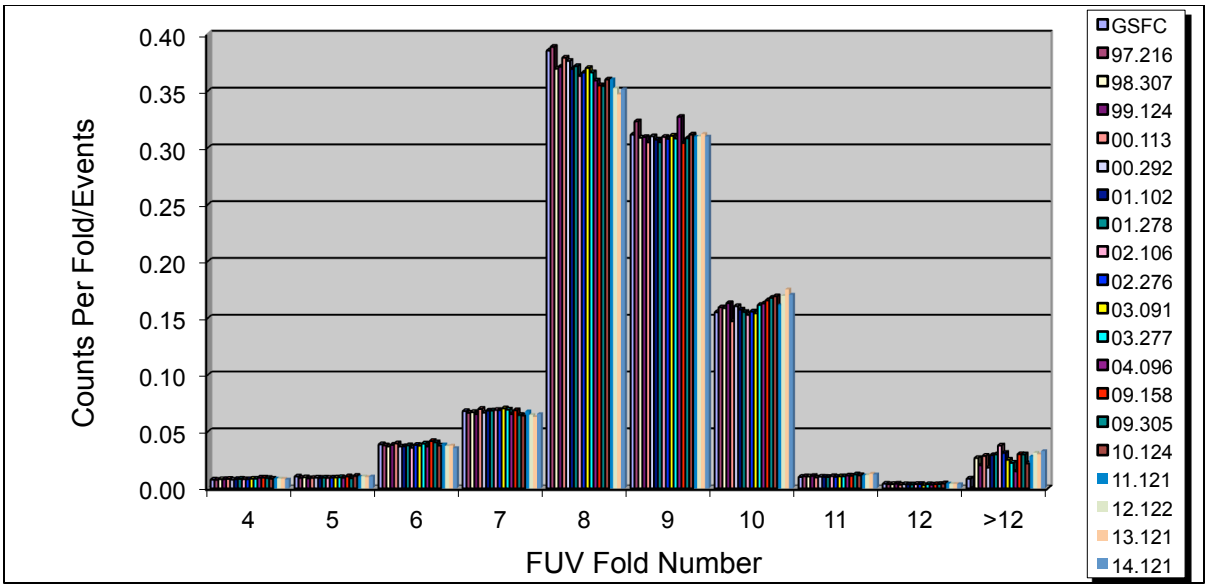

Figure 37. FUV MAMA Fold Histogram

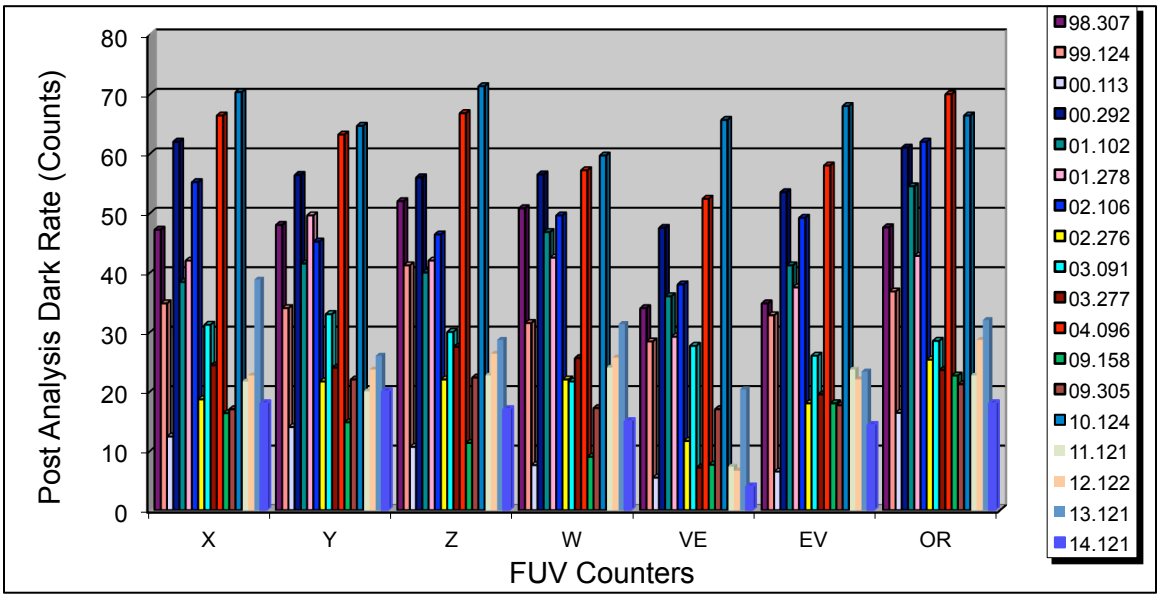

Figure 38. FUV MAMA Post-Test Dark Count Histogram

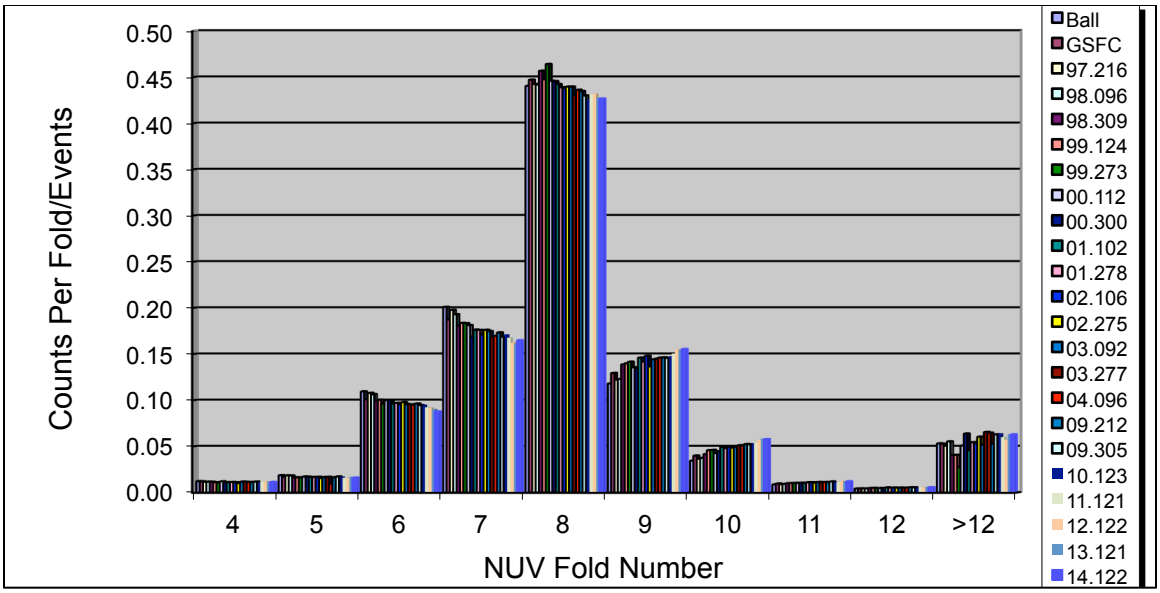

Figure 39. NUV MAMA Fold Histogram

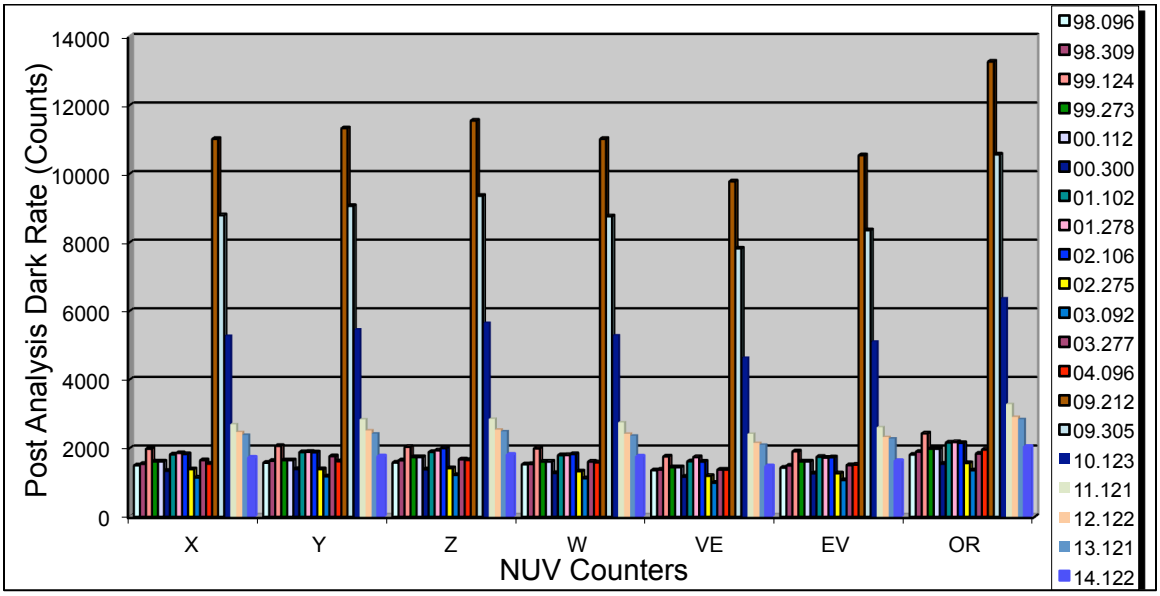

Figure 40. NUV MAMA Fold Histogram

Proposal ID 13545: STIS CCD Saturation Limits Cycle 21

(PI: Charles Proffitt)

Analysis Lead, Others: Charles Proffitt

Summary of Goals and program design

The purpose of this program was to measure, as a function of position on the detector, the level at which individual STIS CCD pixels stop responding linearly to added photons. Tests were done at both GAIN=1 and GAIN=4 at a variety of detector positions. At each position and gain, several HITM1 CCD MIRVIS lamp exposures at exposures levels ranging from ~ 0.4X to 2X full well were taken, using the 0.09X29 aperture. Non-standard MSM positions were used to image this slit at five different rows along the detector. At each of these rows, two different mirror tilts were used to allow this narrow aperture to cover the full width of the detector.

Execution: All visits executed successfully between Dec 30, 2013 and June 30, 2014

Summary of Analysis and Results

For each region of the CCD detector, the local saturation limit can be found by determining where the peak pixel in an image no longer increases linearly with the exposure time. An example of this behavior for our data is shown in Figure 41. Comparing the peak pixel in each column of the narrow stripes illuminated by our lamp exposures allows the local satuaration limit to be mapped as a function of position on the detector (Figure 42).

The originally documented full well depth for the STIS CCD with GAIN=4 was 144,000 e^- near the center of the detector (Kimble et al. 1998), with an ~20% roll-off towards the detector edges. The results we find here suggest that for observations near or below the central row of the detector, the actual local linearity limit is about 128,000 e^- near the central columns dropping to as low as 108,000 e^- near the left and right edges. This same pattern appears to apply in the entire lower half of the detector, at least between rows 128 and 514. However, in the upper part of the detector near the E1 position at row 900, the local pixel response remains linear up to values as large as 160,000 e^-, with little or no roll-off towards the left and right edges. While the results near row 707 show an intermediate behavior, the exact mapping of full well depth in the transition region between rows 514 and 707 remains poorly defined.

For GAIN=4, when the local image intensity begins to exceed about 160,000 e^-, serial transfer artifacts also begin to appear. The origin of these features is likely in the CCD readout electronics, rather than in the detector chip itself. These serial artifacts limit the linearity beyond saturation as summing in the vertical direction no longer recovers all of the incident events. Observers relying on this behavior as reported by Gilliland et al. (1999) should keep their targets close to the central rows of the detector.

For the GAIN=1 setting we find the same full well limit of about 33,000 DN as was reported by Kimble et al. (1998). Further details are presented in the Instrument Science Report by Proffitt (2015).

Accuracy Achieved: Quoted linearity limits should be accurate to approximately 1000 DN.

Reference Files Delivered: None

Relevant ISRs: ISR STIS 2015-03, "STIS CCD Saturation Effects", by C.R. Proffitt

Continuation Plans

None, although future observations might usefully probe the GAIN=4 linearity limits between rows 515 and 707 where we found a dramatic change in behavior.

Supporting Details

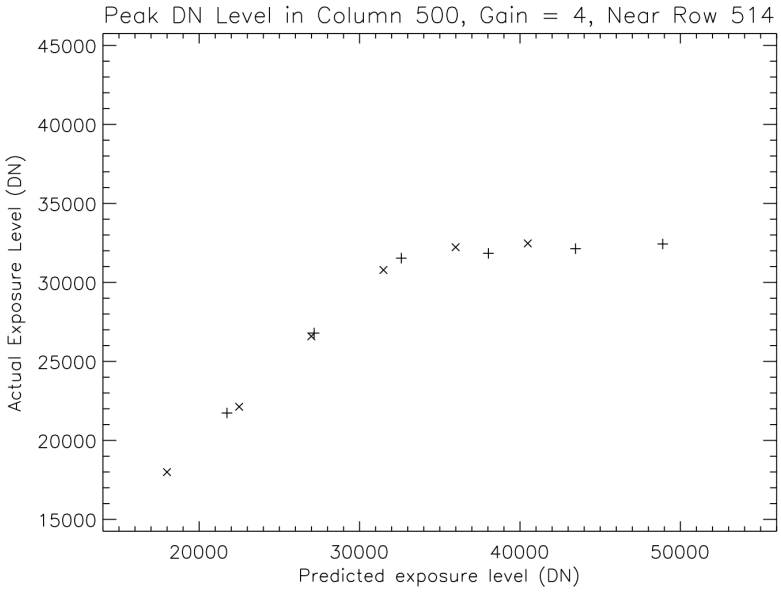

Figure 41. For each of a series of GAIN=4 exposures centered near row 514, we compare the value of the peak pixel in column 500 to the value predicted by scaling the shortest exposure at that position to each actual exposure time. Both the left and right offset exposures overlap this column. The X's show values for the exposures shifted right by +240 pixels in X, while the +'s are for the observations shifted left by −251. In this location, the response begins to flatten at a level of about 32000 DN.

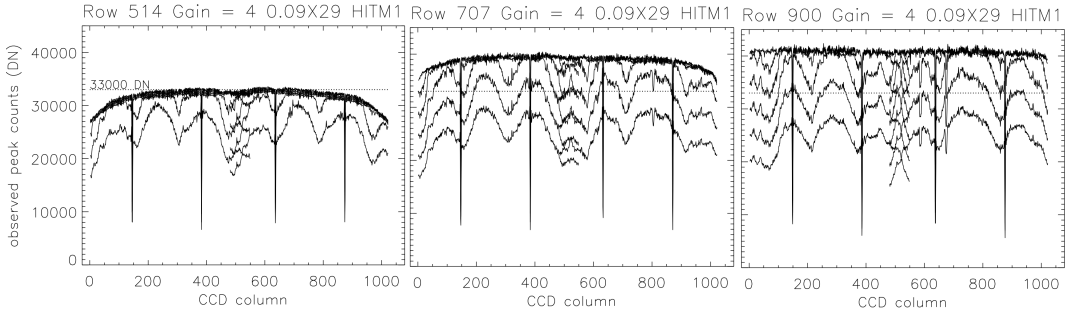

Figure 42. The peak pixel value in each column of the FLT files produced from a series of GAIN=4 STIS CCD HITM1 exposures of increasing length taken through the 0.09X31 aperture are shown. As the local saturation limit is approached, the peak value no longer increases linearly with the exposure time. For reference, the dotted horizontal line marks the 33000 DN (132500 e-) level. The response was also checked near rows 128 and 321 where values for the local saturation limit very similar to those seen at row 512 were found.

References

Gilliland, R. L., Goudfrooij, P, & Kimble, R. A. 1999, PASP, 111, 1009
Kimble, R. A., et al. 1998, ApJL, 492, L83
Proffitt, C. R. 2015, ISR STIS 2015-03, STIS CCD Saturation Effects, STIS (STScI: Baltimore)